Power Electronic Systems
Laboratory

IEEE Journal of Emerging and Selected Topics in Power Electronics, Vol. 8, No. 2, pp. 1833-1849, June 2020

Enhanced Complex Space Vector Modeling and Control System Design of Multiphase Magnetically Levitated Rotary-Linear Machines

S. Miric,
R. Giuffrida,
D. Bortis,
J. W. Kolar

Eidgenössische Technische Hochschule Zürich
Swiss Federal Institute of Technology Zurich

Enhanced Complex Space Vector Modeling and Control System Design of Multiphase Magnetically Levitated Rotary-Linear Machines

Spasoje Mirić, *Student Member, IEEE*, Rosario Giuffrida, *Student Member, IEEE*, Dominik Bortis, *Member, IEEE*, and Johann W. Kolar, *Fellow, IEEE*

***Abstract*—Rotary-linear electric machines can perform coupled rotary and linear motion. Additionally, they can have magnetic bearings (MBs) integrated and magnetically coupled with the rotary, linear or rotary-linear machine operation. Since rotary-linear machines with MBs have not been thoroughly analyzed in literature, the models that provide understanding of their operation and give basis for the control system implementation are not entirely covered. Hence, in this paper an enhanced complex space vector based model of the rotary-linear machine with MBs is derived and expressions for the torque, thrust force and MB force are given. The rotary-linear machine complex space vector of the voltage, current or flux linkage, is defined using the proposed transformation with two complex frames, one related to the rotation and MBs and another to the linear motion. This results in complex space vectors with two complex units, however, the techniques used for a conventional complex space vector calculation can also be applied to the proposed complex space vector description. This is also experimentally validated on a hardware prototype of a magnetically levitated linear tubular actuator (MALTA), whose position control system is designed and implemented based on the enhanced space vector modeling approach, with the dynamic operation of the MALTA including linear motor operation with a axial stroke of 10 mm and mechanical frequency of 17 Hz.**

***Index Terms*—Active Magnetic Bearings, Complex Space Vector, Multiphase Machine, Rotary-Linear Motor, Synchronous Machine.**

I. Introduction

The actuators that can achieve rotary, linear or coupled rotary-linear motion are used in many versatile applications [1] such as pick-and-place robots [2], [3], active suspension systems [4], compressors [5], wave energy harvesting [6], to mention a few. One of the main parts that limits the performance of the rotary-linear actuators are the bearings. Most of the conventional actuators use mechanical bearings, either ball or slider bearings. These bearings introduce drawbacks such as particle generation and the need for lubrication, which is a limiting factor for purity sensitive applications. In high-precision applications ($\sim$ nm range), the thermal expansions of the mechanical bearings limit the precision of the system and make it temperature dependent. Moreover, mechanical bearings limit the lifetime of the actuator [7]. In order to partially overcome these issues, in some applications air bearings are used [8], [9], which on the other hand increase the system complexity due to the needed external air supply and the operation in low pressure environments is not possible. All the above mentioned issues may be solved with magnetic bearings (MBs) [10], which are already largely employed in high-purity [11], high-speed applications [12], ultra high-speed systems [13] or nanometer precision planar actuators [14]. However, the usage of MBs in rotary-linear actuator systems has not been thoroughly studied in literature. In [15] and [16], tubular linear actuators with separate and integrated MBs are shown, but mainly focusing on the magnetic design without extensive details about the models used for control system design and implementation. In [16], the integration of the two machines (the linear and the rotary MB machine) results in a winding similar to the magnetically coupled rotary-linear machine winding [17]. Such a machine, having the winding used for the magnetic levitation that is at the same time magnetically coupled with the linear motion, requires a decoupling transformation that clearly indicates the current components contributing only to the MB forces or only to the thrust force. Only in this case, an independent and decoupled control of the mentioned forces can be achieved. Therefore, in this paper an enhanced complex space vector model is derived which allows to control any rotary-linear machine with/without MB based on only one space vector, which is actually rotating in two complex planes, one for the rotary and one for the linear movement. This model may also directly be applied to a linear machine with integrated MBs [16], which is a special case of the rotary-linear machine with zero rotational speed. Moreover, in order to easily follow the derivations, standard complex space vector models of the rotary and linear machines with and without MBs are revisited and a general three-phase machine model used throughout the paper is established. To the authors best knowledge, for the first time in the literature, a complex space vector of the coupled rotary-linear machine is formulated and used to explain the torque, thrust force and the magnetic bearing force generation principles.

In **Sec. II** the complex space vector models of the rotary machine, rotary machine with MBs, linear machine, rotary-linear machine, rotary-linear machine with MBs and the linear

This work was supported by ETH Research Grant ETH-13 16-2. Moreover, the authors acknowledge the support of CADFEM (Suisse) AG concerning the ANSYS software. Warm thanks also go to Fabian Dietschi for implementing the initial control system firmware.

All authors are with the Power Electronic Systems Laboratory, Swiss Federal Institute of Technology (ETH) Zurich, 8092 Zurich, Switzerland (S. Mirić is the corresponding author, e-mail: miric@lem.ee.ethz.ch).

machine with MBs are established. In **Sec. III** a linear machine with integrated MBs, also called MALTA (MAgnetically Levitated Tubular Actuator) is further investigated. Namely, its winding that has drive and bearing current components (called *combined winding*) causes peculiar arrangement of these components where the drive currents act as zero-sequence currents from the bearing currents stand point of view. In **Sec. IV** the realization of the MALTA hardware and the control system design and implementation are described. Finally, in **Sec. V**, the decoupled control achieved with the enhanced complex space vector modeling is verified with experimental measurements obtained from the existing prototype. **Sec. VI** concludes the paper and gives an outlook.

II. Complex Space Vector Model

In general, complex space vector theory may be used to model symmetric, asymmetric, sinusoidal and non-sinusoidal steady state and transient phenomena of three-phase electric machines [18]. Mainly, it is developed to describe the transient behavior of electric machines, where traditional single-phase equivalent circuit can not be used [19]. Especially in modern actuator systems, where electric machines rarely operate in steady-state sinusoidal regime with constant amplitude and electrical frequency of the supply voltage. For the first time, the space vector theory was introduced in [20] and their purpose was to model alternating current (AC) machines in direct online drives. Today, in modern industry, complex space vector theory is used to model three-phase systems, such that in three-phase power converters, which are either connected to a three-phase electric grid [21] or to a three-phase electric machine [22]–[26], the phase currents and voltages are properly controlled. Compared to the other approaches, e.g. generalized machine theory where pure mathematical formalism is applied and an electric machine is viewed 'from outside' as 'black box', with electric currents at the input and torque and/or force at the output, space vector theory allows to view machine 'from inside' and model spacial field distribution in the air gap [27].

Based on this, in this section the complex space vector models of three-phase electric machines, focusing on the magnetic coupling of the rotary and linear motion [17] with MBs, are derived. In order to introduce a general three-phase electric machine model, the derivation starts with the conventional rotary machine and develops further towards the rotary-linear machine with MBs.

For the sake of clarity, i and j are used to denote complex units of the two different complex planes related to rotation/magnetic levitation and linear motion, respectively. For the notation of electric currents always either indices or the complex space vector notation $\underline{i}$ or $\underline{\underline{i}}$ is used.

A. Rotary Machine: Torque

An example of a three-phase electric machine with 6 teeth in the stator and 8 poles in the rotor is shown in **Fig. 1**. For different machines these numbers may differ, but they would still have a three-phase system in the stator. In order to simplify and generalize the analysis of three-phase electric machines, a

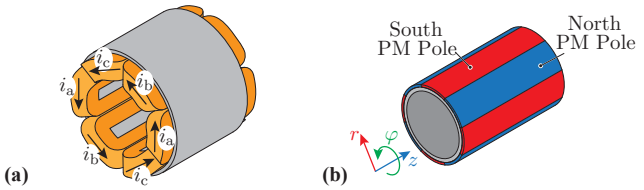

(a) (b)

Fig. 1: An example of a rotary machine realization with **(a)** 6 concentrated coils in the stator and **(b)** 8 poles in the rotor, i.e. the number of the pole pairs is $N_{\mathrm{pp,R}} = 4$. The mechanical rotational speed of the rotor is Ω_{mech}, and it is related to the electrical angular speed as $\omega_{\mathrm{R}} = N_{\mathrm{pp,R}}\Omega_{\mathrm{mech}}$.

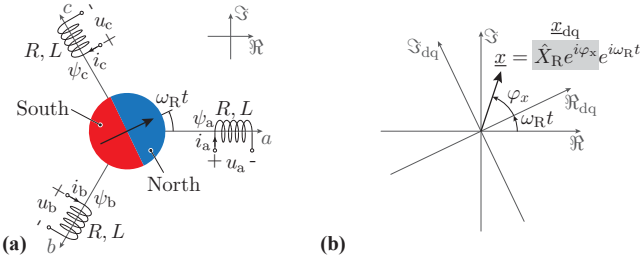

(a) (b)

Fig. 2: **(a)** The three-phase electric machine model with the 3 coils spatially displaced by 120° and the 2-pole rotor. The mechanical rotational speed of the rotor is equal to the electrical angular speed of the modeled machine (for the rotary machine ω_{R}). **(b)** The complex space vector machine model represented either in the stationary reference frame $(\Re, \Im)$ or in the rotary reference frame $(\Re_{\mathrm{dq}}, \Im_{\mathrm{dq}})$.

model with 3 stator coils and a 2-pole rotor is used, as shown in **Fig. 2(a)**. It should be noted that this model can resemble concentrated and distributed stator windings, with or without iron teeth, i.e. slotted or slotless windings, which are spatially displaced by 120°. Furthermore, also the electrical quantities such as the voltages on the terminals $u_{\{\mathrm{a,b,c}\}}$, the currents in the coils $i_{\{\mathrm{a,b,c}\}}$ and the flux linkages of the coils $\psi_{\{\mathrm{a,b,c}\}}$ are shifted by 120° in time (cf. **Fig. 2(a)**). These quantities are described by their amplitude $\hat{X}_{\mathrm{R}}$ and phase $\omega_{\mathrm{R}}t + \varphi_x$ as

$$\begin{bmatrix} x_{\mathrm{a}} \\ x_{\mathrm{b}} \\ x_{\mathrm{c}} \end{bmatrix} = \hat{X}_{\mathrm{R}} \cdot \begin{bmatrix} \cos\left(\omega_{\mathrm{R}}t + \varphi_x + \gamma_{\mathrm{a}}\right) \\ \cos\left(\omega_{\mathrm{R}}t + \varphi_x + \gamma_{\mathrm{b}}\right) \\ \cos\left(\omega_{\mathrm{R}}t + \varphi_x + \gamma_{\mathrm{c}}\right) \end{bmatrix}, \tag{1}$$

where x can be any of the quantities u, i or ψ denoted as $x \in \{u, i, \psi\}$ with the amplitude $\hat{X}_{\mathrm{R}} \in \{\hat{U}_{\mathrm{R}}, \hat{I}_{\mathrm{R}}, \hat{\Psi}_{\mathrm{R}}\}$. The initial phase angle is given as φ_x while $\gamma_{\mathrm{a}} = 0°$, $\gamma_{\mathrm{b}} = -120°$ and $\gamma_{\mathrm{c}} = 120°$ are the electrical angles that determine the three-phase system, where the three phases for the rotation are denoted with lowercase letters as 'a', 'b' and 'c'. For symmetric electric machines, the sum of the quantities is equal to zero, i.e. $x_{\mathrm{a}} + x_{\mathrm{b}} + x_{\mathrm{c}} = 0$. Consequently, the three-phase system $\{x_{\mathrm{a}}, x_{\mathrm{b}}, x_{\mathrm{c}}\}$ is determined by knowing only 2 out of 3 quantities (e.g. if the first two quantities are given, the third one is $x_{\mathrm{c}} = -x_{\mathrm{a}} - x_{\mathrm{b}}$). This allows to model the three-phase system in a two-dimensional coordinate system, i.e. the complex plane $(\Re, \Im)$, which is extensively used in the analysis of three-phase electric machines. As shown in **Fig. 2(a)**, the complex plane $(\Re, \Im)$ is superimposed to the general three-phase electric machine model. Based on that, a complex space vector may be defined using the positions

of the coils in the model and the instantaneous values of the three-phase quantities as

$$\underline{x} \triangleq \frac{2}{3}\begin{bmatrix}1 & \underline{a} & \underline{a}^2\end{bmatrix}\begin{bmatrix}x_\mathrm{a}\\ x_\mathrm{b}\\ x_\mathrm{c}\end{bmatrix} \tag{2}$$

where $\underline{a} = e^{i(2\pi/3)}$ is a complex number and i the imaginary unit. This results in a space vector rotating in the complex plane $(\Re, \Im)$ which fully describes the three-phase quantities present in the windings. The amplitude of the space vector is the magnitude $|\underline{x}| = \hat{X}_\mathrm{R}$ and its argument equals the phase of the quantities $\arg(\underline{x}) = \omega_\mathrm{R} t + \varphi_x$, which is graphically represented in **Fig. 2(b)**. This can be directly seen by writing the space vector in its exponential form $\underline{x} = \hat{X} e^{i\varphi_x} e^{i\omega_\mathrm{R} t}$. The instantaneous values of the quantities are again simply obtained as $x_\mathrm{a} = \Re\{\underline{x}\}$, $x_\mathrm{b} = \Re\{\underline{a}^2\,\underline{x}\}$ and $x_\mathrm{c} = \Re\{\underline{a}\,\underline{x}\}$.

The space vector model of the three-phase electric machine can be further simplified by its representation in the rotary complex frame $(\Re_\mathrm{dq}, \Im_\mathrm{dq})$, also known as 'dq' frame. The complex space vector in the 'dq' frame rotating with the angular frequency ω_R removes the electrical angular speed from its representation and it is equal to $\underline{x}_\mathrm{dq} = \underline{x}\, e^{-i\omega_\mathrm{R} t} = \hat{X} e^{i\varphi_x}$ (cf. **Fig. 2(b)**). Its real and imaginary components ($\underline{x}_\mathrm{dq} = x_\mathrm{d} + i x_\mathrm{q}$) are known as 'dq' components and are related to the amplitude and phase angle as $\hat{X}_\mathrm{R} = \sqrt{x_\mathrm{d}^2 + x_\mathrm{q}^2}$ and $\varphi_x = \mathrm{atan2}(x_\mathrm{q}/x_\mathrm{d})$, where atan2 is the function that calculates the angle between the $\underline{x}_\mathrm{dq}$ and the 'd' axis considering also the periodicity between $\pm\pi/2$ of the tangent function [28].

In summary, the three-phase electric machine quantities may be represented either with the three-phase electric machine model shown in **Fig. 2(a)** in combination with the system of equations given in (1), or with the complex space vector model from **Fig. 2(b)**, which is equal to $\underline{x}$ in the stationary complex frame or $\underline{x}_\mathrm{dq}$ in the rotary reference frame.

The established three-phase electric machine complex space vector representation may also be used to determine the mechanical torque T_z of the machine. For this purpose, in the first step the instantaneous input electric power is determined. By using the three-phase quantities given in (1), the instantaneous electrical power is calculated as $p_\mathrm{el} = \sum_{k=\{a,b,c\}} u_k i_k$. The same power may be obtained by using the complex space vectors of the voltage and current as $p_\mathrm{el} = \Re\{3/2\,\underline{u}\,\underline{i}^*\} = \Re\{3/2\,\underline{u}_\mathrm{dq}\,\underline{i}^*_\mathrm{dq}\}$, where * denotes the conjugate complex number. In both cases, it is necessary to determine the voltage equation. The three-phase model will have 3 voltage equations (i.e. one equation per coil), which can be put together into a single complex space vector equation by using the transformation defined in (2) as

$$\underline{u} = R\underline{i} + L\frac{d\underline{i}}{dt} + \frac{d\underline{\psi}}{dt}, \tag{3}$$

where R is the resistance of the coils and L is the inductance (cf. **Fig. 2(a)**). It should be noted that the mutual inductance between the coils in **Fig. 2(a)** is neglected in order to have a clearer presentation, but can be easily included while (3) would have the same form. By using (3), the electric power is equal to

$$p_\mathrm{el} = \frac{3}{2} R \hat{I}_\mathrm{R}^2 + \frac{3}{2} L\, \Re\left\{\frac{d\underline{i}}{dt}\underline{i}^*\right\} + \frac{3}{2}\Re\left\{\frac{d\underline{\psi}}{dt}\underline{i}^*\right\}. \tag{4}$$

The first term $3/2\, R\hat{I}_\mathrm{R}^2$ models the copper losses in the stator winding, the second term $3/2\, L\, \Re\{d\underline{i}/dt\, \underline{i}^*\}$ represents the power used to change the magnetic energy in the machine, while the third term $3/2\, \Re\{d\underline{\psi}/dt\, \underline{i}^*\}$ is further analyzed. The space vector of the flux linkage $\underline{\psi}$ can be expressed as $\underline{\psi} = \hat{\Psi}_\mathrm{R} e^{i\varphi_\psi} e^{i\omega_\mathrm{R} t} = (\psi_\mathrm{d} + i\psi_\mathrm{q}) e^{i\omega_\mathrm{R} t}$. Usually, the rotating complex frame, the 'dq' frame, is positioned such that the 'd' axis $\Re_\mathrm{dq}$ coincides with the flux linkage space vector $\underline{\psi}$, which leads to $\varphi_\psi = 0°$ (cf. **Fig. 2(b)**). Therefore, the flux linkage space vector in the stationary complex frame is $\underline{\psi} = \hat{\Psi}_\mathrm{R} e^{i\omega_\mathrm{R} t}$, while in the rotary 'dq' frame $\underline{\psi}_\mathrm{dq} = \psi_\mathrm{d} = \hat{\Psi}_\mathrm{R}$. Similarly, the conjugate complex space vector of the current in the stationary complex frame is $\underline{i}^* = (\underline{i}_\mathrm{dq} e^{i\omega_\mathrm{R} t})^* = \underline{i}^*_\mathrm{dq} e^{-i\omega_\mathrm{R} t}$, where the complex conjugate in the 'dq' frame is $\underline{i}^*_\mathrm{dq} = i_\mathrm{d} - i\, i_\mathrm{q}$. Using these expressions for $\underline{\psi}$ and $\underline{i}^*$, the third term of (4) is further developed as

$$\frac{3}{2}\Re\left\{\frac{d\underline{\psi}}{dt}\underline{i}^*\right\} = \frac{3}{2}\frac{d\hat{\Psi}_\mathrm{R}}{dt} i_\mathrm{d} + \omega_\mathrm{R}\frac{3}{2}\hat{\Psi}_\mathrm{R}\, i_\mathrm{q}, \tag{5}$$

where the first term only results when also a change in the flux linkage magnitude $\hat{\Psi}_\mathrm{R}$ is considered. Hence, this term represents the power necessary to change the flux linkage $\hat{\Psi}_\mathrm{R}$, e.g. used for field weakening operation of the electric machine and may be changed with the 'd' component of the current i_d. The second term represents the mechanical power of the machine, which at the shaft is equal to $p_\mathrm{mech} = \Omega_\mathrm{mech} T_\mathrm{z}$, where Ω_mech is the mechanical rotational speed of the rotor in $\mathrm{rad\,s^{-1}}$ and T_z is the mechanical torque. Having in mind the relation of the electrical angular speed and the mechanical speed $\omega_\mathrm{R} = N_\mathrm{pp,R}\Omega_\mathrm{mech}$, where $N_\mathrm{pp,R}$ is the number of pole pairs in the rotor, the mechanical torque is equal to

$$T_\mathrm{z} = \frac{3}{2} N_\mathrm{pp,R}\, \hat{\Psi}_\mathrm{R} i_\mathrm{q}. \tag{6}$$

Therefore, the mechanical torque is controlled by the 'q' current component (i_q).

B. Rotary Machine: Bearing Force

Rotary machines are mainly used to generate torque, but may also be used to generate the bearing force if the winding configuration, i.e. the interconnection between several phase windings is accordingly adjusted. For a given number of stator teeth and pole pairs $N_\mathrm{pp,R}$ in the rotor, the winding configuration for the torque generation can be optimized and is well documented in literature [29] and there are even online tools for the winding configuration calculation [30]. For the bearing force generation the same winding arrangement as for the torque generation can be used, while only the winding interconnections have to be reconfigured. This actually results in a different virtual number of pole pairs of the stator winding, which means that depending on the winding interconnection a different stator field harmonic is pronounced

by the three-phase currents. For example, if the number of the pole pairs in the rotor is $N_{\mathrm{pp,R}}$, the winding configuration optimized for the torque generation with $N_{\mathrm{pp,B}} = N_{\mathrm{pp,R}} \pm 1$ pole pairs should be used to generate the bearing force. In literature, this is known as the self-bearing motor $N_{\mathrm{pp,R}} \pm 1$ type [10], [31]. To show this in an example, the winding configuration of the machine shown in **Fig. 1**, which has concentrated windings with 6 teeth and a rotor with $N_{\mathrm{pp,R}} = 4$, is analyzed and reconfigured, i.e. changing the interconnection of phase windings, such that the rotary machine can also generate the bearing force. Hence, in order to generate torque, the stator winding should be connected such that the three-phase currents in the coils have directions as denoted in **Fig. 1(a)**, which can be represented with the set as $W_{\mathrm{T}} = \{i_{\mathrm{a}}, i_{\mathrm{b}}, i_{\mathrm{c}}, i_{\mathrm{a}}, i_{\mathrm{b}}, i_{\mathrm{c}}\}$. As already mentioned, to use the same winding for the bearing force generation, a winding configuration for $N_{\mathrm{pp,B}} = 4 \pm 1$ pole pairs should be used. Since it is not possible to have a concentrated winding with 6 teeth and 3 pole pairs [30], a winding configuration that is able to generate $N_{\mathrm{pp,B}} = 5$ pole pairs has to be used, which in this case means that the coils are connected as $W_{\mathrm{B}} = \{i_{\mathrm{a}}, -i_{\mathrm{b}}, i_{\mathrm{c}}, -i_{\mathrm{a}}, i_{\mathrm{b}}, -i_{\mathrm{c}}\}$. In contrast to W_{T}, the winding configuration W_{B} actually means that now the two corresponding phase windings are connected in anti-series instead of being connected in series, thus by applying the three-phase currents to the rotary electric machine shown in **Fig. 1**, with the W_{B} winding configuration the bearing force onto the rotor is generated.

In order to control the magnetic bearing forces (F_{x} and F_{y}), a three-phase model of the magnetic bearing machine similar to the one shown in **Fig. 2(a)** is established. The difference between the torque machine winding and the bearing machine winding is that now due to this anti-series connection of the phase windings the overall flux linkage in the bearing winding, i.e. the sum of the flux linked with both phase coils, is equal to 0 when the rotor is in its center position, i.e. when there is no radial displacement of the rotor, $x = 0$ and $y = 0$, independent from the angular position of the rotor. A nonzero flux linkage in the bearing winding only appears when a radial displacement of the rotor is present. To model this, the coils in the three-phase electric machine model from **Fig. 2(a)** are split in half, placed from both sides of the rotor and are connected in anti-series as shown in **Fig. 3(a)**. As will be explained in the following, with this arrangement the total flux linkage in all coils becomes nonzero when the rotor is displaced from the center, i.e. $x \neq 0$ and/or $y \neq 0$, and can be calculated as

$$\begin{aligned}\psi_{\{\mathrm{a,b,c}\}} = &\frac{d\hat{\Psi}_{\mathrm{R}}}{dx} x \cos(\omega_{\mathrm{R}} t + \varphi_{\psi} + \{\gamma_{\mathrm{a}}, \gamma_{\mathrm{b}}, \gamma_{\mathrm{c}}\}) - \\ &\frac{d\hat{\Psi}_{\mathrm{R}}}{dy} y \sin(\omega_{\mathrm{R}} t + \varphi_{\psi} + \{\gamma_{\mathrm{a}}, \gamma_{\mathrm{b}}, \gamma_{\mathrm{c}}\}),\end{aligned} \tag{7}$$

where $d\hat{\Psi}_{\mathrm{R}}/dx$ and $d\hat{\Psi}_{\mathrm{R}}/dy$ are the change of the flux linkage with respect to the radial displacement. The deduction of this radial displacement-dependent flux linkage given in (7) is explained for phase 'a' based on **Fig. 3(b-d)**.

In a first step, a displacement x in $x-$direction is assumed, while the rotor flux is also pointing in positive $x-$direction. As shown in **Fig. 3(b)**, a displacement in positive $x-$direction

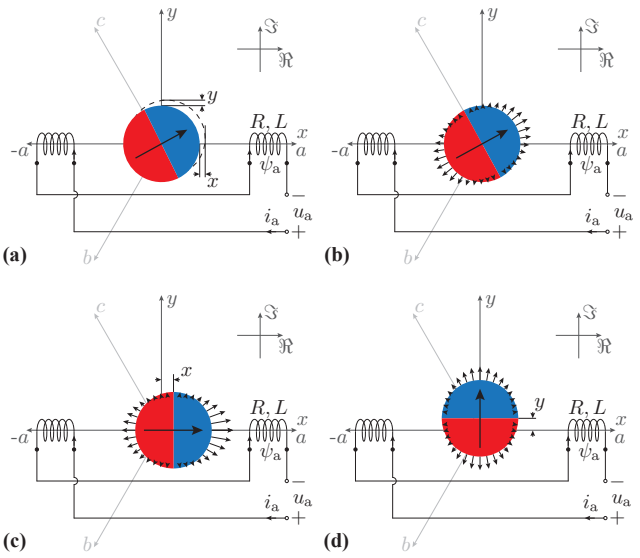

Fig. 3: **(a)** The three-phase electric machine bearing force model where a radial displacement of the rotor in $x-$ and $y-$direction is allowed. It is derived from the three-phase machine model shown in **Fig. 2(a)** by splitting the coils in half, placing them from both sides of the rotor and connecting them in anti-series. This allows to model the bearing winding, in which the flux linkage only exists when the rotor is displaced from its center. **(b)** Radial flux density component of the rotor PMs. The rotor is in the center and, therefore, the flux linkage of the first phase $\psi_{\mathrm{a}} = 0$. **(c)** The rotor is displaced in $x-$direction by x with the rotary orientation $(\omega_{\mathrm{R}} t + \varphi_{\psi}) = 0$. Assuming the constant sensitivity $d\hat{\Psi}_{\mathrm{R}}/dx$, the flux linkage of the first phase is $\psi_{\mathrm{a}} = (d\hat{\Psi}_{\mathrm{R}}/dx)\, x$. **(d)** The rotor is displaced in y direction by y with the rotary orientation $(\omega_{\mathrm{R}} t + \varphi_{\psi}) = \pi/2$. Assuming the constant sensitivity $d\hat{\Psi}_{\mathrm{R}}/dy$, the flux linkage of the first phase is $\psi_{\mathrm{a}} = -(d\hat{\Psi}_{\mathrm{R}}/dy)\, y$.

leads to an increased flux linkage in the right coil, while the flux linkage with the left coil is reduced, thus the total flux linkage with both coils is increasing. Assuming a certain constant sensitivity $d\hat{\Psi}_{\mathrm{R}}/dx = \chi_{\mathrm{pm,x}}$ the resulting flux linkage can be calculated as $(d\hat{\Psi}_{\mathrm{R}}/dx)\, x = \chi_{\mathrm{pm,x}}\, x$. As can be noticed, however, this is only true when the rotor's angular position is equal to $(\omega_{\mathrm{R}} t + \varphi_{\psi}) = 0°$. If e.g. the rotor is rotated by 180°, the flux linkage would be the same as with 0°, but in the negative direction, which means a multiplication by -1. Furthermore, at the angular positions 90° and 270° a displacement in $x-$direction ideally does not result in any total flux linkage. Consequently, the arbitrary rotational position of the rotor (cf. **Fig. 3(c)**) has to be considered, which for an $x-$displacement can be done by multiplying $(d\hat{\Psi}_{\mathrm{R}}/dx)\, x = \chi_{\mathrm{pm,x}}\, x$ with $\cos(\omega_{\mathrm{R}} t + \varphi_{\psi} + \gamma_{\mathrm{a}})$.

In analogy to the x displacement, the influence of a y displacement can be analyzed. As it may be imagined based on **Fig. 3(d)**, when the rotor flux is pointing in $y-$direction, the resulting flux linkage is $(-d\hat{\Psi}_{\mathrm{R}}/dy)\, y = -\chi_{\mathrm{pm,y}}\, y$, if again a certain constant sensitivity $d\hat{\Psi}_{\mathrm{R}}/dy = \chi_{\mathrm{pm,y}}$ is assumed. Furthermore, the flux linkage again depends on the rotating position, which for a y displacement has to be considered with $\sin(\omega_{\mathrm{R}} t + \varphi_{\psi} + \gamma_{\mathrm{a}})$ and thus leads to the second term of (7). By applying now the transformation given in (2) and assuming that $\chi_{\mathrm{pm,x}} = \chi_{\mathrm{pm,y}} = \chi_{\mathrm{pm,R}}$, the complex space

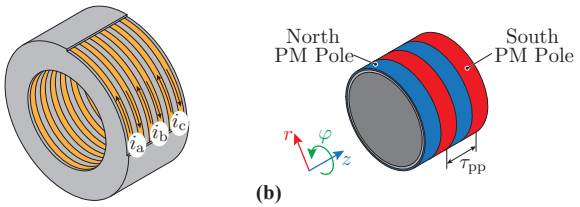

(a) **(b)**

Fig. 4: (a) A three-phase electric linear machine stator realization with 6 teeth single layer winding. **(b)** Rotor (also called 'mover' for linear machines) with 4 poles. The pole pair width (twice the pole pitch) is denoted as τ_{pp}.

vector of the bearing flux linkage in the stationary complex frame is obtained

$$\underline{\psi} = \chi_{\mathrm{pm,R}}\,(x+iy)\,e^{i\varphi_\psi}e^{i\omega_{\mathrm{R}}t}, \tag{8}$$

where x and y equal the radial displacements [32]. The complex space vector of the flux linkage in the rotary 'dq' frame is $\underline{\psi}_{\mathrm{dq}} = \chi_{\mathrm{pm,R}}\,(x+iy)\,e^{i\varphi_\psi}$. Since the rotating 'dq' frame is positioned such that $\varphi_\psi = 0$, the complex space vector of the flux linkage is then equal to $\underline{\psi}_{\mathrm{dq}} = \chi_{\mathrm{pm,R}}\,(x+iy)$.

To obtain the expressions for the mechanical bearing forces F_{x} and F_{y}, similar as for the mechanical torque, the expression of the instantaneous electric power p_{el} is analyzed. The electric power may be obtained by using the complex space vectors as $p_{\mathrm{el}} = \Re\{3/2\,\underline{u}\,\underline{i}^*\} = \Re\{3/2\,\underline{u}_{\mathrm{dq}}\,\underline{i}^*_{\mathrm{dq}}\}$, which results in the same expression found in (4). Accordingly, for the mechanical bearing force analysis only the last term given in (4) is needed, which leads to

$$\begin{aligned}\frac{3}{2}\Re\left\{\frac{d\underline{\psi}}{dt}\underline{i}^*\right\} =& \frac{3}{2}\chi_{\mathrm{pm,R}}\left(v_{\mathrm{x}}i_{\mathrm{d}} + v_{\mathrm{y}}i_{\mathrm{q}}\right) + \\ & \frac{3}{2}\chi_{\mathrm{pm,R}}\,\omega_{\mathrm{R}}\left(xi_{\mathrm{q}} - yi_{\mathrm{d}}\right),\end{aligned} \tag{9}$$

where $v_{\mathrm{x}} = dx/dt$ and $v_{\mathrm{y}} = dy/dt$ are the rotor velocities in $x-$ and $y-$direction. The total mechanical power with the allowed radial displacement of the rotor is $p_{\mathrm{mech}} = v_{\mathrm{x}}\,F_{\mathrm{x}} + v_{\mathrm{y}}\,F_{\mathrm{y}} + \Omega_{\mathrm{mech}}T_{\mathrm{z}}$. Comparing the terms of p_{mech} with the terms in (9), the bearing forces are

$$F_{\mathrm{x}} = \frac{3}{2}\chi_{\mathrm{pm,R}}\,i_{\mathrm{d}}, \qquad F_{\mathrm{y}} = \frac{3}{2}\chi_{\mathrm{pm,R}}\,i_{\mathrm{q}}. \tag{10}$$

As can be noted, the radial force components can be independently controlled with i_{d} and i_{q} current components of the bearing winding. In addition, there is a parasitic torque created when the rotor radial displacement is nonzero, which is equal to $T_{\mathrm{z}} = (3/2)\,N_{\mathrm{pp,R}}\,\chi_{\mathrm{pm,R}}\,(xi_{\mathrm{q}} - yi_{\mathrm{d}})$ and has to be compensated by the controller.

C. Linear Machine: Thrust Force

An example of the three-phase electric linear machine realization is shown in **Fig. 4**. It should be noted that instead of the pole pair number for the rotary machine, the pole pair width τ_{pp} is given for the linear machine.

From the perspective of the electrical machine analysis, the three-phase linear electric machine is similar to the rotary machine, i.e. the stator winding is characterized by the three-phase voltage, current and the flux linkage

$$\begin{bmatrix} x_{\mathrm{A}} \\ x_{\mathrm{B}} \\ x_{\mathrm{C}} \end{bmatrix} = \hat{X}_{\mathrm{L}} \cdot \begin{bmatrix} \cos\left(\omega_{\mathrm{L}}t + \theta_x + \gamma_{\mathrm{A}}\right) \\ \cos\left(\omega_{\mathrm{L}}t + \theta_x + \gamma_{\mathrm{B}}\right) \\ \cos\left(\omega_{\mathrm{L}}t + \theta_x + \gamma_{\mathrm{C}}\right) \end{bmatrix}, \tag{11}$$

where $\hat{X}_{\mathrm{L}} \in \{\hat{U}_{\mathrm{L}}, \hat{I}_{\mathrm{L}}, \hat{\Psi}_{\mathrm{L}}\}$ is the amplitude, ω_{L} is the linear machine electrical angular speed, θ_x is the phase angle and $\gamma_{\mathrm{A}} = 0°$, $\gamma_{\mathrm{B}} = -120°$ and $\gamma_{\mathrm{C}} = 120°$ are the electrical angles that determine the three-phase system, where the three phases for linear motion are denoted with uppercase letters as 'A', 'B' and 'C'. Therefore, the same model from **Fig. 2** may be used for the linear machine analysis. In the rotary machine the rotational mechanical speed Ω_{mech} is related to the electrical angular speed ω_{R}, while for the linear machine the linear mechanical speed v_{z} is related to the linear machine electrical angular speed as

$$\omega_{\mathrm{L}} = \frac{2\pi}{\tau_{\mathrm{pp}}}\,v_{\mathrm{z}}. \tag{12}$$

Similar to the rotary machine, where the electrical power is analyzed based on (4) to get the expression for the mechanical torque, for the linear machine the same expression can be used, just with the linear machine quantities. Therefore, the last term of (4) is

$$\frac{3}{2}\Re\left\{\frac{d\underline{\psi}}{dt}\underline{i}^*\right\} = \frac{3}{2}\frac{d\hat{\Psi}_{\mathrm{L}}}{dt}\,i_{\mathrm{d}} + \omega_{\mathrm{L}}\frac{3}{2}\hat{\Psi}_{\mathrm{L}}\,i_{\mathrm{q}}, \tag{13}$$

where $\hat{\Psi}_{\mathrm{L}}$ is the flux linkage of the linear machine. The first term again describes the magnetic power to change the flux linkage (flux weakening), while the second term is related to the mechanical output power. By using (12) and the mechanical power $p_{\mathrm{mech}} = v_{\mathrm{z}}F_{\mathrm{z}}$, the thrust force is obtained as

$$F_{\mathrm{z}} = \frac{3\pi}{\tau_{\mathrm{pp}}}\hat{\Psi}_{\mathrm{L}}i_{\mathrm{q}} \tag{14}$$

In analogy to the mechanical torque obtained in a rotary machine, the thrust force is controlled by the 'q' current component i_{q}.

D. Linear Machine: Bearing Force

In order to generate and control the bearing force onto the rotor of a linear machine, the air gap flux density has to be controlled around the rotor circumference such that a 'radial pull' is created in the desired direction. However, the three-phase linear machine has a winding that is circumferentially homogeneous (cf. **Fig. 4(a)**). Consequently, the air gap flux density around the circumference cannot be adjusted with the linear machine winding. Therefore, the conventional linear machine cannot be used as a bearing machine.

E. Rotary-Linear Machine: Torque + Thrust Force

A rotary-linear machine may be realized by coupling a rotary and a linear machine either mechanically or magnetically. The analysis of the rotary-linear machine with the mechanical coupling may be split into the separate analyses of the rotary and linear machines explained in **Sec. II-A** and **Sec. II-C**,

respectively. The analysis of the rotary-linear machine with the magnetic coupling is clarified in this section. A realization example of such a machine is shown in **Fig. 5**. Since the stator windings have to be able to generate torque and thrust force at the same time, concentrated stator coils are needed, which can be seen as a combination of the winding arrangements used for the rotary machine (denoted with lowercase letters {a,b,c}) and the linear machine (denoted with uppercase letters {A,B,C}). As illustrated in **Fig. 5(a)**, the concentrated coils of the rotary-linear machine resemble the rotary machine in rotary direction and the linear machine in linear direction. Similarly, the rotor's PM arrangement results from a combination of the PM arrangement needed for the rotary machine and the linear machine, which leads to a checkerboard-type PM arrangement (cf. **Fig. 5(b)**). Therefore, the number of pole pairs in rotary direction is again $N_{\mathrm{pp,R}}$, and the pole pair width in linear direction is τ_{pp}.

Finally, also the voltages and currents which have to be applied to the magnetically coupled rotary-linear machine windings can be seen as a combination of the quantities needed for the rotary machine and the linear machine. Compared to a conventional rotary machine, for example, this means that for the rotary-linear machine also a rotating flux density has to be generated by the stator windings in order to produce torque, however, in this case also the linear position of the rotor has to be considered, since for each rotary three-phase winding set (e.g. {aA, bA, cA} compared to {aB, bB, cB}) the PM alignment below each three-phase winding set is different and therefore different torque-generating currents have to be injected into the rotary three-phase windings. Accordingly, the same is also true in linear direction, which means that for the generation of thrust force, for each linear three-phase winding set (e.g. {aA, aB, aC} compared to {bA, bB, bC}) the rotation angle has to be considered, since the PM alignment for each linear three-phase winding set is different. This can be achieved by multiplying the rotary three-phase quantities (e.g. $\cos(\omega_{\mathrm{R}}t)$) with the linear three-phase quantities (e.g. $\cos(\omega_{\mathrm{L}}t)$), which corresponds to a modulation of the rotary quantities in linear direction with the electrical angular speed ω_{L} and a modulation of the linear quantities in rotary direction with the electrical angular speed ω_{R}. Therefore, the phase quantities of the rotary-linear machine have the following form

$$x_{\{\mathrm{a,b,c}\}\{\mathrm{A,B,C}\}} = \hat{X}_{\mathrm{RL}} \cos\left(\omega_{\mathrm{R}}t + \varphi_x + \{\gamma_{\mathrm{a}}, \gamma_{\mathrm{b}}, \gamma_{\mathrm{c}}\}\right) \times \cos\left(\omega_{\mathrm{L}}t + \theta_x + \{\gamma_{\mathrm{A}}, \gamma_{\mathrm{B}}, \gamma_{\mathrm{C}}\}\right), \tag{15}$$

where $\hat{X}_{\mathrm{RL}} \in \{\hat{U}_{\mathrm{RL}}, \hat{I}_{\mathrm{RL}}, \hat{\Psi}_{\mathrm{RL}}\}$ is the amplitude, φ_x is the rotary initial phase angle and θ_x is the linear initial phase angle. It should be noted again that the lowercase letters $\{\mathrm{a,b,c}\}$ denote the rotary component, while the uppercase letters $\{\mathrm{A,B,C}\}$ denote the linear component.

In order to unify the analysis of the rotary-linear machines and apply the same techniques as for the rotary and linear machines, the complex space vector of the magnetically coupled rotary-linear machine is defined. Hence, two complex planes are needed, one for the rotary component (with the complex unit i) and another for the linear component (with the complex unit j). The complex space vector for the magnetically coupled rotary-linear machine is defined with the following transformation

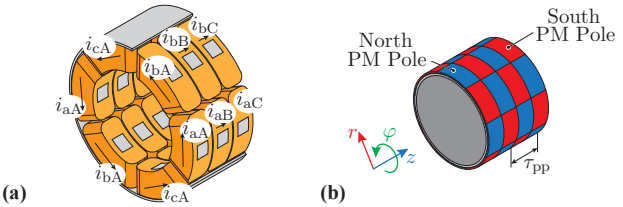

Fig. 5: (a) A rotary-linear machine stator realization with 6 teeth for the rotation and 3 teeth for the linear motion. **(b)** The rotor of the rotary-linear machine with $N_{\mathrm{pp,R}} = 4$ pole pairs for the rotation and with a pole pair width of τ_{pp} for the linear motion.

$$\underline{\underline{x}} \triangleq \frac{4}{9}\begin{bmatrix}1 & \underline{a} & \underline{a}^2\end{bmatrix}\begin{bmatrix}x_{\mathrm{aA}} & x_{\mathrm{aB}} & x_{\mathrm{aC}} \\ x_{\mathrm{bA}} & x_{\mathrm{bB}} & x_{\mathrm{bC}} \\ x_{\mathrm{cA}} & x_{\mathrm{cB}} & x_{\mathrm{cC}}\end{bmatrix}\begin{bmatrix}1 \\ \underline{b} \\ \underline{b}^2\end{bmatrix}, \tag{16}$$

where $\underline{\underline{x}} \in \{\underline{\underline{u}}, \underline{\underline{i}}, \underline{\underline{\psi}}\}$, $\underline{a} = e^{i(2\pi/3)}$ and $\underline{b} = e^{j(2\pi/3)}$ are complex numbers. It should be noted that the 'double underline' $\underline{\underline{x}}$ denotes the complex space vector with the two different complex units. This results in the space vector rotating simultaneously in two complex planes, $(\Re^i, \Im^i)$ and $(\Re^j, \Im^j)$, and fully describing the phase quantities of the rotary-linear machine. The amplitude of the complex space vector is the magnitude $|\underline{\underline{x}}| = \hat{X}_{\mathrm{RL}}$ and its arguments are the rotary and linear phases of the phase quantities, i.e. $\arg^i(\underline{\underline{x}}) = \omega_{\mathrm{R}}t + \varphi_x$ and $\arg^j(\underline{\underline{x}}) = \omega_{\mathrm{L}}t + \theta_x$. This can be seen by writing the complex space vector in its exponential form as

$$\underline{\underline{x}} = \underbrace{\hat{X}_{\mathrm{RL}}e^{i\varphi_x}e^{j\theta_x}}_{\underline{\underline{x}}_{\mathrm{dq}}} e^{i\omega_{\mathrm{R}}t}e^{j\omega_{\mathrm{L}}t}, \tag{17}$$

where $\underline{\underline{x}}_{\mathrm{dq}}$ is the complex space vector in the double-rotary 'dq'-frame. The defined complex space vector (16) has 4 components

$$\underline{\underline{x}}_{\mathrm{dq}} = x_{\mathrm{dd}} + ix_{\mathrm{qd}} + jx_{\mathrm{dq}} + ijx_{\mathrm{qq}}, \tag{18}$$

which may be obtained by applying the Euler's formula (e.g. $e^{i\omega_{\mathrm{R}}t} = \cos(\omega_{\mathrm{R}}t) + i\sin(\omega_{\mathrm{R}}t)$) on each of the exponents in (17). The first index of each component belongs to the rotary and the second index to the linear machine. Accordingly, the component x_{dd} equals in both complex planes, i.e. for the rotary and linear machine, to a real component and thus in both complex planes is pointing in $d-$direction. The component ix_{qd} is purely imaginary for the rotary machine (first index 'q') and purely real for the linear machine (second index 'd'), while for the component jx_{qd} it is exactly opposite. Finally, the component ijx_{qq} is a component which in both complex planes is purely imaginary, therefore in both frames points in $q-$direction.

In order to obtain instantaneous values given with (15) from the complex space vector $\underline{\underline{x}}$, a similar procedure as for the complex space vector $\underline{x}$ is applied. Namely, depending on the desired instantaneous component ($x_{\{\mathrm{a,b,c}\}\{\mathrm{A,B,C}\}}$) the complex space vector is multiplied at first with either $1, a, a^2, b$

and/or b^2 and then the real part $\Re$ is taken, which can be written as

$$\begin{bmatrix} x_{\mathrm{aA}} & x_{\mathrm{aB}} & x_{\mathrm{aC}} \\ x_{\mathrm{bA}} & x_{\mathrm{bB}} & x_{\mathrm{bC}} \\ x_{\mathrm{cA}} & x_{\mathrm{cB}} & x_{\mathrm{cC}} \end{bmatrix} = \Re \left\{ \begin{bmatrix} 1 \\ \underline{a}^2 \\ \underline{a} \end{bmatrix} \underline{\underline{x}} \begin{bmatrix} 1 & \underline{b}^2 & \underline{b} \end{bmatrix} \right\}. \quad (19)$$

After defining the complex space vector of the rotary-linear machine, further calculations are similar as for the rotary or linear machines. Hence, in order to obtain the expressions for the torque and the thrust force of the rotary-linear machine, again the power balance, i.e. the conversion from electrical input power to mechanical output power, is analyzed. The input electrical power is the sum of the powers of each phase, which can be written using the double sum operators $p_{\mathrm{el}} = \sum_{m=\{a,b,c\}} \sum_{n=\{A,B,C\}} u_{mn} i_{mn}$. It also can be calculated using the complex space vectors as $p_{\mathrm{el}} = \Re\{9/4\, \underline{\underline{u}}\, \underline{\underline{i}}^*\} = \Re\{9/4\, \underline{\underline{u}}_{\mathrm{dq}}\, \underline{\underline{i}}^*_{\mathrm{dq}}\}$, which together with the voltage space vector equation given in (3) results in

$$p_{\mathrm{el}} = \frac{9}{4} R \hat{I}^2_{\mathrm{RL}} + \frac{9}{4} L\, \Re \left\{ \frac{d\underline{\underline{i}}}{dt} \underline{\underline{i}}^* \right\} + \frac{9}{4} \Re \left\{ \frac{d\underline{\underline{\psi}}}{dt} \underline{\underline{i}}^* \right\}. \quad (20)$$

Similar to the analysis of the electric power expression for the rotary machine (cf. (4)), the first two terms do not contribute to the mechanical power but consider either the losses in the windings or the change in magnetic energy. Therefore, the third term $9/4\, \Re \left\{ d\underline{\underline{\psi}}/dt\, \underline{\underline{i}}^* \right\}$ is further analyzed. As the 'dq' frames are oriented in such a way that $\varphi_\psi = 0$ and $\theta_\psi = 0$, the complex space vector of the flux linkage is then equal to $\underline{\underline{\psi}} = \hat{\Psi}_{\mathrm{RL}} e^{i\omega_{\mathrm{R}} t} e^{j\omega_{\mathrm{L}} t}$. The conjugate complex space vector of the current is equal to $\underline{\underline{i}}^* = \hat{I}_{\mathrm{RL}} e^{-i\varphi_i} e^{-j\theta_i} e^{-i\omega_{\mathrm{R}} t} e^{-j\omega_{\mathrm{L}} t} = \underline{\underline{i}}^*_{\mathrm{dq}}\, e^{-i\omega_{\mathrm{R}} t} e^{-j\omega_{\mathrm{L}} t}$, where $\underline{\underline{i}}^*_{\mathrm{dq}} = i_{\mathrm{dd}} - i i_{\mathrm{qd}} - j i_{\mathrm{dq}} + ij i_{\mathrm{qq}}$. Using these expressions, the last term in (20) is equal to

$$\frac{9}{4} \Re \left\{ \frac{d\underline{\underline{\psi}}}{dt} \underline{\underline{i}}^* \right\} = \frac{9}{4} \frac{d\hat{\Psi}_{\mathrm{RL}}}{dt} i_{\mathrm{dd}} + \omega_{\mathrm{R}} \frac{9}{4} \hat{\Psi}_{\mathrm{RL}} i_{\mathrm{qd}} + \omega_{\mathrm{L}} \frac{9}{4} \hat{\Psi}_{\mathrm{RL}} i_{\mathrm{dq}}. \quad (21)$$

The first term is the power used to change the flux linkage $\hat{\Psi}_{\mathrm{RL}}$, e.g. used for field weakening. The other two terms correspond to the mechanical power of the rotation and the linear motion. Considering the expression for the total mechanical power obtained at the shaft $p_{\mathrm{mech}} = \Omega_{\mathrm{mech}} T_{\mathrm{z}} + v_{\mathrm{z}} F_{\mathrm{z}}$ and the ratios between the electrical and mechanical angular speeds $\omega_{\mathrm{R}} = N_{\mathrm{pp,R}} \Omega_{\mathrm{mech}}$ and $\omega_{\mathrm{L}} = 2\pi/\tau_{\mathrm{pp}}\, v_{\mathrm{z}}$, the torque and the thrust force are calculated as

$$T_{\mathrm{z}} = \frac{9}{4} N_{\mathrm{pp,R}} \hat{\Psi}_{\mathrm{RL}}\, i_{\mathrm{qd}}, \qquad F_{\mathrm{z}} = \frac{9\pi}{2\tau_{\mathrm{pp}}} \hat{\Psi}_{\mathrm{RL}}\, i_{\mathrm{dq}}. \quad (22)$$

As can be noted, the mechanical torque and the thrust force in the rotary-linear machine can be fortunately controlled with two independent current components i_{qd} and i_{dq}, which for the corresponding machine part, i.e. rotary or linear machine, equals to the $q-$current (torque or force generation) and in the other machine part results in a $d-$component (field weakening/amplification). It should be mentioned that this result agrees with the torque and the thrust force expressions derived in [17].

F. Rotary-Linear Machine: Bearing Force

Similar to the rotary machine discussed in **Sec. II-B**, the bearing force may also be generated with the rotary-linear machine. In analogy to the rotary machine, for the rotary-linear machine the winding configuration has to be adjusted. Consequently, in order to generate the torque, the winding configuration in rotary direction is $W_{\mathrm{T}} = \{i_{\mathrm{a}X}, i_{\mathrm{b}X}, i_{\mathrm{c}X}, i_{\mathrm{a}X}, i_{\mathrm{b}X}, i_{\mathrm{c}X}\}$, where '$X$' in the index denotes any of the linear phase components $X \in \{\mathrm{A}, \mathrm{B}, \mathrm{C}\}$, and to generate the bearing force, the winding configuration in rotary direction should be $W_{\mathrm{B}} = \{i_{\mathrm{a}X}, -i_{\mathrm{b}X}, i_{\mathrm{c}X}, -i_{\mathrm{a}X}, i_{\mathrm{b}X}, -i_{\mathrm{c}X}\}$ (cf. **Sec. II-B**).

The flux linkage modeling considerations are similar as for the rotary machine given with (7) and shown in **Fig. 3**, while for the rotary-linear machine in addition to the rotation angle, which is already considered in (7), also the linear position of the rotor has to be taken into account. Hence, (7) has to be multiplied with $\cos\left(\omega_{\mathrm{L}} t + \theta_\psi + \{\gamma_{\mathrm{A}}, \gamma_{\mathrm{B}}, \gamma_{\mathrm{C}}\}\right)$, which in other words corresponds to a modulation of the flux linkage in linear direction, and results in the following expression

$$\begin{aligned} \psi_{\{\mathrm{a,b,c}\}\{\mathrm{A,B,C}\}} = \chi_{\mathrm{pm,RL}} \Big(& x \cos(\omega_{\mathrm{R}} t + \varphi_\psi + \{\gamma_{\mathrm{a}}, \gamma_{\mathrm{b}}, \gamma_{\mathrm{c}}\}) - \\ & y \sin(\omega_{\mathrm{R}} t + \varphi_\psi + \{\gamma_{\mathrm{a}}, \gamma_{\mathrm{b}}, \gamma_{\mathrm{c}}\}) \Big) \times \\ & \cos\left(\omega_{\mathrm{L}} t + \theta_\psi + \{\gamma_{\mathrm{A}}, \gamma_{\mathrm{B}}, \gamma_{\mathrm{C}}\}\right), \end{aligned} \quad (23)$$

where $\chi_{\mathrm{pm,RL}}$ is the flux linkage radial sensitivity of the rotary-linear machine. By applying the proposed complex space vector transformation for the rotary-linear machines (cf. (16)), the bearing flux linkage vector is

$$\underline{\underline{\psi}} = \chi_{\mathrm{pm,RL}}\, (x + iy)\, e^{i\varphi_\psi} e^{j\theta_\psi} e^{i\omega_{\mathrm{R}} t} e^{j\omega_{\mathrm{L}} t}. \quad (24)$$

The complex space vectors of the voltage $\underline{\underline{u}}$ and the current $\underline{\underline{i}}$ are the same as for the rotary-linear machine (cf. (17)).

To determine the bearing forces F_{x} and F_{y} of the rotary-linear machine, similar to the previous analysis for the rotary machine, the expressions for the electrical and mechanical powers are used. The electric power may be calculated using the complex space vectors (cf. (20)). Similar as for the torque and the thrust force calculation, the last term in (20) is further analyzed

$$\begin{aligned} \frac{9}{4} \Re \left\{ \frac{d\underline{\underline{\psi}}}{dt} \underline{\underline{i}}^* \right\} = & \frac{9}{4} \chi_{\mathrm{pm,RL}} \Big(v_{\mathrm{x}} i_{\mathrm{dd}} + v_{\mathrm{y}} i_{\mathrm{qd}} + \\ & \omega_{\mathrm{R}} (x i_{\mathrm{qd}} - y i_{\mathrm{dd}}) + \omega_{\mathrm{L}} (x i_{\mathrm{dq}} + y i_{\mathrm{qq}}) \Big), \end{aligned} \quad (25)$$

where $v_{\mathrm{x}} = dx/dt$, $v_{\mathrm{y}} = dy/dt$, $\omega_{\mathrm{R}} = N_{\mathrm{pp,R}} \Omega_{\mathrm{mech}}$ and $\omega_{\mathrm{L}} = 2\pi/\tau_{\mathrm{pp}} v_{\mathrm{z}}$. The mechanical power is equal to $p_{\mathrm{mech}} = v_{\mathrm{x}} F_{\mathrm{x}} + v_{\mathrm{y}} F_{\mathrm{y}} + v_{\mathrm{z}} F_{\mathrm{z}} + \Omega_{\mathrm{mech}} T_{\mathrm{z}}$. By comparing these coefficients with (25), the bearing forces of the rotary-linear machine are obtained as

$$F_{\mathrm{x}} = \frac{9}{4} \chi_{\mathrm{pm,RL}}\, i_{\mathrm{dd}}, \qquad F_{\mathrm{y}} = \frac{9}{4} \chi_{\mathrm{pm,RL}}\, i_{\mathrm{qd}}. \quad (26)$$

Again, the radial force components of the rotary-linear machine can be independently controlled with i_{dd} and i_{qd} current components of the bearing winding, which

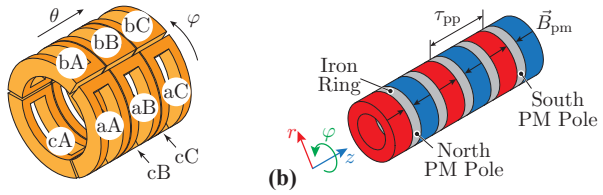

Fig. 6: **(a)** Stator winding arrangement of the MALTA with 9 phase windings. **(b)** The MALTA rotor is similar to the rotor of a linear machine (cf. **Fig. 4**). Due to simpler manufacturing, the MALTA rotor has axially magnetized PMs in combination with iron rings.

in both cases means that the bearing forces are generated with the linear $d-$current component. In addition, there are parasitic torque and thrust force components created when the rotor radial displacement is nonzero. They are equal to $T_\mathrm{z} = (9/4)\, N_\mathrm{pp,R}\, \chi_\mathrm{pm,RL}\, (x i_\mathrm{qd} - y i_\mathrm{dd})$ and $F_\mathrm{z} = (9\pi/2\tau_\mathrm{pp})\, \chi_\mathrm{pm,RL}\, (x i_\mathrm{dq} + y i_\mathrm{qq})$ and have to be compensated by the controller.

G. Linear Machine: Thrust Force + Bearing Force

As shown in **Sec. II-D**, the linear machine analyzed in **Sec. II-C** cannot generate any bearing forces and, therefore, cannot be operated as a self-bearing machine.

In contrast, the linear machine analyzed in this section can be operated as a self-bearing machine and can be derived either from the standard linear machine shown in **Fig. 4**, by interrupting the linear machine winding in circumferential direction and creating the three new coils as shown in **Fig. 6(a)**, or from the rotary-linear machine discussed in the previous section. Hence, the resulting machine is a combination of a rotary-linear machine winding and a linear machine rotor (cf. **Fig. 6**).

This machine type, also called MALTA (MAgnetically Levitated Tubular Actuator), is for the first time proposed in [16], where the magnetic design and hardware realization are discussed.

The achievable thrust and the bearing forces of the MALTA are determined by using the complex space vector models derived for the linear and rotary-linear machines. It should be noted that they are first analyzed separately, i.e. it is assumed that the MALTA winding is carrying only the thrust force current or only the bearing force current, which in the literature is known as separate winding arrangement [33]. In a second step, the superposition of the thrust and bearing force currents is analyzed in **Sec. III**.

1) MALTA Thrust Force Generation: From the thrust force generation point of view, the MALTA winding (cf. **Fig. 6(a)**) behaves the same as the winding of the linear machine analyzed in **Sec. II-C** (cf. **Fig. 4(a)**). Therefore, the currents in the MALTA winding are equal in circumferential (rotary) direction, i.e. $i_{\mathrm{a}X} = i_{\mathrm{b}X} = i_{\mathrm{c}X}$, where $X \in \{\mathrm{A}, \mathrm{B}, \mathrm{C}\}$. Consequently, it is enough to analyze one third (one circumferential third) of the MALTA winding (e.g. coils $\{\mathrm{aA}, \mathrm{aB}, \mathrm{aC}\}$). Accordingly, the findings can afterwards also be applied to the rest of the windings.

Furthermore, the analysis concerning thrust force, which was conducted for the linear machine (cf. **Sec. II-C**) can also be applied to one third of the MALTA winding. Therefore, the phase quantities in MALTA responsible for the thrust force will have the same waveform as the ones for the linear machine (cf. (11)). After transforming the three-phase currents into the rotating 'dq' frame, the i_q current component will contribute to the thrust force generation as $3\pi/\tau_\mathrm{pp}\, \hat{\Psi}_\mathrm{M} i_\mathrm{q}$, where τ_pp is the pole pair width in the MALTA rotor (cf. **Fig. 6(b)**) and $\hat{\Psi}_\mathrm{M}$ is the flux linkage of the MALTA coil. However, since only one third of the MALTA winding is considered, the total thrust force of the MALTA is obtained by multiplying the linear machine force expression by 3, which gives

$$F_\mathrm{z} = \frac{9\pi}{\tau_\mathrm{pp}} \hat{\Psi}_\mathrm{M}\, i_\mathrm{q}. \tag{27}$$

This expression is verified with measurements on the MALTA prototype [16]. The term $(9\pi/\tau_\mathrm{pp})\, \hat{\Psi}_\mathrm{M}$ represents the MALTA thrust force constant. The pole pair width in the MALTA prototype is $\tau_\mathrm{pp} = 30\,\mathrm{mm}$ and the measured flux linkage is $\hat{\Psi}_\mathrm{M} = 8.35\,\mathrm{mWb}$. By using these two values, the MALTA thrust force constant is calculated to be $(9\pi/\tau_\mathrm{pp})\, \hat{\Psi}_\mathrm{M} = 7.8\,\mathrm{N\,A^{-1}}$. On the other hand, using the external force sensor in the test bench, the value of the MALTA thrust force constant is measured to be $7.6\,\mathrm{N\,A^{-1}}$ (cf. (6) in [16]). The calculated and the measured value differ by $\approx 2.6\,\%$, which verifies (27).

2) MALTA Bearing Force Generation: The generation of the bearing forces in the MALTA is very similar to the rotary-linear machine analyzed in **Sec. II-F**. The waveforms of the MALTA bearing voltage and current match with (15), while only $\omega_\mathrm{R} = 0$. Applying the transformation (16), the complex space vector of the voltage and the current is

$$\underline{\underline{x}} = \hat{X}_\mathrm{M,b} e^{i\varphi_x} e^{j\theta_x}\, e^{j\omega_\mathrm{L} t} = \underline{\underline{x}}_\mathrm{dq}\, e^{j\omega_\mathrm{L} t} \tag{28}$$

where $x \in \{u, i\}$ and $\underline{\underline{x}}_\mathrm{dq} = \hat{X}_\mathrm{M,b} e^{i\varphi_x} e^{j\theta_x}$. Similarly, for the flux linkage, (23) may be used, where $\omega_\mathrm{R} = 0$. With (16) this results in the complex space vector of the MALTA bearing flux linkage as

$$\underline{\underline{\psi}} = \chi_\mathrm{pm,M}\, (x + iy)\, e^{i\varphi_\psi} e^{j\theta_\psi} e^{j\omega_\mathrm{L} t}, \tag{29}$$

where $\chi_\mathrm{pm,M}$ is the MALTA flux linkage radial sensitivity. In order to determine the bearing forces F_x and F_y of the MALTA, similar to the rotary-linear machine, the electric power and the mechanical power expressions are compared. The term of the electric power that contributes to the mechanical power is the same as for the rotary-linear machine (cf. (25)), just replacing $\omega_\mathrm{R} = 0$. Therefore, the radial forces of the MALTA are generated as

$$F_\mathrm{x} = \frac{9}{4} \chi_\mathrm{pm,M}\, i_\mathrm{dd}, \qquad F_\mathrm{y} = \frac{9}{4} \chi_\mathrm{pm,M}\, i_\mathrm{qd}, \tag{30}$$

which are same bearing forces as obtained in (26) and are again independently controlled with the i_dd and i_qd current components of the MALTA winding. In addition, a parasitic thrust force component is created when the rotor radial displacement is nonzero, which is equal to $F_\mathrm{z} = (9\pi/2\tau_\mathrm{pp}) \chi_\mathrm{pm,M}\, (x i_\mathrm{dq} + y i_\mathrm{qq})$ and has to be compensated by the controller.

In order to verify (30) and to estimate the impact of the parasitic thrust force, the flux linkage radial sensitivity for the MALTA prototype from [16] is estimated with FEM. For the MALTA prototype, where each coil has 205 turns, the average flux linkage radial sensitivity is $\chi_{\mathrm{pm,M}} \approx 2.56\,\mathrm{Wb\,m^{-1}}$. Using (30), the term $(9/4)\,\chi_{\mathrm{pm,M}} \approx 5.75\,\mathrm{N\,A^{-1}}$ is the MALTA average bearing constant, since the effective value also depends on the displacement direction, i.e. whether the rotor is displaced either towards a stator tooth or towards the stator winding, as explained and measured in [16]. The average thrust force constant is then $5.94\,\mathrm{N\,m^{-1}}$, which is very close to the value calculated using (30). The value for the flux linkage radial sensitivity $\chi_{\mathrm{pm,M}}$ may also be used to check for the expected parasitic thrust force. For the MALTA prototype $\tau_{\mathrm{pp}} = 30\,\mathrm{mm}$ and if a radial displacement of $x = 10\,\mu\mathrm{m}$ and an electrical current of $i_{\mathrm{dq}} = 6\,\mathrm{A}$ are assumed, the parasitic thrust force is calculated to be $F_{\mathrm{z}} = (9\pi/2\tau_{\mathrm{pp}})\chi_{\mathrm{pm,M}}\,(x i_{\mathrm{dq}} + y i_{\mathrm{qq}}) = 0.07\,\mathrm{N}$, which is negligible compared to the MALTA continuous forces $\sim 20\,\mathrm{N}$ (cf. [16]). For the sake of clarity, the assumed current $i_{\mathrm{dq}} = 6\,\mathrm{A}$ is double the continuous current allowed by the thermal limit, and only occurs e.g. during transients.

III. MALTA with Combined Windings

After deriving the force and torque generation from the enhanced complex space vector modeling for all different kind of machine realizations, now the proposed modeling concept is verified based on a hardware prototype of a MALTA with combined windings. In general, in electric machines that can generate torque and/or thrust force in combination with magnetic bearing force, the windings are realized either as separate or combined windings [33], [34]. The separated winding arrangement contains a drive winding dedicated to the torque and/or thrust force generation and a bearing winding dedicated to the bearing force generation (i.e. a bearing winding). On the other hand, the combined winding has only one winding, where the drive and bearing currents are superimposed. Usually, the separated winding is more difficult to manufacture than the combined winding, as the two different winding systems have to be implemented onto the same magnetic core. On the other hand, with the separated winding the control system implementation is simpler compared to the combined winding, as the drive and bearing quantities (voltages, currents and flux linkages) are inherently decoupled.

Nevertheless, the MALTA used as an example in this paper is realized with combined winding, since it mainly offers benefits concerning the hardware effort, e.g. the number of phase legs and switches in the inverter, and due to the fact that the copper cross-section is better utilized with combined windings. Consequently, the two components of the voltage, current and the flux linkage, the drive component (for the thrust force generation) and the bearing component (for the magnetic bearing force generation) are superimposed to each other, and the MALTA phase quantities may be written in the following form

$$\mathbf{X}_{\mathrm{abc}} = \begin{bmatrix} x_{\mathrm{A}} + x_{\mathrm{aA}} & x_{\mathrm{B}} + x_{\mathrm{aB}} & x_{\mathrm{C}} + x_{\mathrm{aC}} \\ x_{\mathrm{A}} + x_{\mathrm{bA}} & x_{\mathrm{B}} + x_{\mathrm{bB}} & x_{\mathrm{C}} + x_{\mathrm{bC}} \\ x_{\mathrm{A}} + x_{\mathrm{cA}} & x_{\mathrm{B}} + x_{\mathrm{cB}} & x_{\mathrm{C}} + x_{\mathrm{cC}} \end{bmatrix}, \tag{31}$$

where $x_{\{\mathrm{A,B,C}\}}$ is the drive component and $x_{\{\mathrm{a,b,c}\}\{\mathrm{A,B,C}\}}$ is the bearing component. According to a conventional linear machine, the drive component of the MALTA phase quantities is equal to

$$x_{\{\mathrm{A,B,C}\}} = \hat{X}_{\mathrm{M}} \cos\left(\omega_{\mathrm{L}} t + \theta_x + \{\gamma_{\mathrm{A}}, \gamma_{\mathrm{B}}, \gamma_{\mathrm{C}}\}\right), \tag{32}$$

where $x \in \{u, i, \psi\}$, $\hat{X}_{\mathrm{M}} \in \{\hat{U}_{\mathrm{M}}, \hat{I}_{\mathrm{M}}, \hat{\Psi}_{\mathrm{M}}\}$ is the drive amplitude, ω_{L} is the electrical angular speed and θ_x is the initial drive phase angle. As can be noted, the drive component results in an offset, i.e. a zero-sequence component, added to the bearing components of each rotary three-phase system (cf. each column in (31)). These zero-sequence components actually appear due to the combined winding, since the stator current in each winding of the MALTA has quantities alternated in two directions, with two electrical angles, rotary φ_x and linear θ_x, cf. (28), and in this case have to be handled carefully using mathematical objects of linear algebra such as vectors and matrices, rather then complex numbers. The bearing component of the MALTA voltage and current quantities is given as

$$x_{\{\mathrm{a,b,c}\}\{\mathrm{A,B,C}\}} = \hat{X}_{\mathrm{Mb}} \cos\left(\varphi_x + \{\gamma_{\mathrm{a}}, \gamma_{\mathrm{b}}, \gamma_{\mathrm{c}}\}\right) \times \cos\left(\omega_{\mathrm{L}} t + \theta_{x,\mathrm{b}} + \{\gamma_{\mathrm{A}}, \gamma_{\mathrm{B}}, \gamma_{\mathrm{C}}\}\right), \tag{33}$$

where $x \in \{u, i\}$, $\hat{X}_{\mathrm{Mb}} \in \{\hat{U}_{\mathrm{Mb}}, \hat{I}_{\mathrm{Mb}}\}$ is the bearing amplitude and φ_x is the direction in which the current space vector has to point in order to counteract the displacement, which together with $\hat{X}_{\mathrm{Mb}}$ is later defined by the bearing current controller. Furthermore, since not all stator windings are facing the same PM in axial direction, the linear position of the rotor has to be considered for the bearing current and voltages, which is achieved by the multiplication with $\cos\left(\omega_{\mathrm{L}} t + \theta_{x,\mathrm{b}} + \{\gamma_{\mathrm{A}}, \gamma_{\mathrm{B}}, \gamma_{\mathrm{C}}\}\right)$ in (33). Hence, the superposition of the three bearing components to the drive component can be interpreted as a redistribution of the drive current to the three radial windings of one linear phase in order to generate bearing forces, while at the same time the average drive component in linear direction is not changed.

As already discussed in **Sec. II-G2**, in contrast to the bearing components of the current and voltage, the bearing component of the flux linkage also depends on the radial displacement. Since for the MALTA there is no dependency on the rotation angle, i.e. $\omega_{\mathrm{R}} t + \varphi_\psi = 0$, based on (23) the flux linkage can be written as

$$\psi_{\{\mathrm{a,b,c}\}\{\mathrm{A,B,C}\}} = \chi_{\mathrm{pm,M}} \left(x \cos\{\gamma_{\mathrm{a}}, \gamma_{\mathrm{b}}, \gamma_{\mathrm{c}}\} - y \sin\{\gamma_{\mathrm{a}}, \gamma_{\mathrm{b}}, \gamma_{\mathrm{c}}\}\right) \times \cos\left(\omega_{\mathrm{L}} t + \theta_\psi + \{\gamma_{\mathrm{A}}, \gamma_{\mathrm{B}}, \gamma_{\mathrm{C}}\}\right), \tag{34}$$

where $\chi_{\mathrm{pm,M}}$ is the MALTA flux linkage radial sensitivity.

A. MALTA Transformation

As shown in **Sec. II-G**, for the MALTA only the currents i_{q}, i_{dd} and i_{qd} have to be controlled to generate the thrust and the bearing force, respectively. Furthermore, as shown in the following, also the i_{d} component must be controlled to zero such that the drive current is kept to a minimum and is not weakening the PM field. Hence, In order to obtain

these quantities, first the 9 MALTA phase quantities ('abc' quantities) have to be transformed into the 9 stationary 'dq0' quantities as

$$\mathbf{X}_{\mathrm{dq0}} = \mathbf{K}_{\mathrm{R0}} \cdot \mathbf{X}_{\mathrm{abc}} \cdot \mathbf{K}_{\mathrm{L0}}, \tag{35}$$

where $\mathbf{K}_{\mathrm{R0}}$ is the rotary electrical angle transformation

$$\mathbf{K}_{\mathrm{R0}} = \frac{2}{3}\begin{bmatrix} \cos\gamma_{\mathrm{a}} & \cos\gamma_{\mathrm{b}} & \cos\gamma_{\mathrm{c}} \\ -\sin\gamma_{\mathrm{a}} & -\sin\gamma_{\mathrm{b}} & -\sin\gamma_{\mathrm{c}} \\ 1/2 & 1/2 & 1/2 \end{bmatrix}, \tag{36}$$

and $\mathbf{K}_{\mathrm{L0}}$ is the linear electrical angle transformation

$$\mathbf{K}_{\mathrm{L0}} = \frac{2}{3}\begin{bmatrix} \cos(\omega_{\mathrm{L}}t+\gamma_{\mathrm{a}}) & -\sin(\omega_{\mathrm{L}}t+\gamma_{\mathrm{a}}) & 1/2 \\ \cos(\omega_{\mathrm{L}}t+\gamma_{\mathrm{b}}) & -\sin(\omega_{\mathrm{L}}t+\gamma_{\mathrm{b}}) & 1/2 \\ \cos(\omega_{\mathrm{L}}t+\gamma_{\mathrm{c}}) & -\sin(\omega_{\mathrm{L}}t+\gamma_{\mathrm{c}}) & 1/2 \end{bmatrix}. \tag{37}$$

It should be noted that these transformation matrices also consider the zero sequence components for rotation and for linear motion, since, as already seen, e.g. the drive component in linear direction is a zero-sequence component for the bearing component (cf. (31)). Hence, the 'dq0' quantities have the following components

$$\mathbf{X}_{\mathrm{dq0}} = \begin{bmatrix} x_{\mathrm{dd}} & x_{\mathrm{dq}} & x_{\mathrm{d0}} \\ x_{\mathrm{qd}} & x_{\mathrm{qq}} & x_{\mathrm{q0}} \\ x_{\mathrm{0d}} & x_{\mathrm{0q}} & x_{\mathrm{00}} \end{bmatrix}, \tag{38}$$

where in the double index notation $x_{\{\mathrm{d,q,0}\}\{\mathrm{d,q,0}\}}$, the first index denotes the respective rotary component ('d', 'q' or '0') while the second index denotes the linear component, i.e. the rows in $\mathbf{X}_{\mathrm{dq0}}$ represent the rotary direction while the columns represent the linear direction. Furthermore, it should be noted that three types of the zero sequence components may be identified: (1) rotary zero sequence components x_{0d} and x_{0q}, (2) linear zero sequence components x_{d0} and x_{q0} and (3) rotary-linear zero sequence component x_{00}. By transforming the 'abc' quantities of the MALTA voltage and the current into the 'dq0' quantities, i.e. inserting (32) and (33) into (31) and applying the transformation given in (35), the following components are obtained

$$\mathbf{X}_{\mathrm{dq0}} = \begin{bmatrix} \hat{X}_{\mathrm{Mb}}\cos\varphi_x\cos\theta_{x,\mathrm{b}} & \hat{X}_{\mathrm{Mb}}\cos\varphi_x\sin\theta_{x,\mathrm{b}} & 0 \\ \hat{X}_{\mathrm{Mb}}\sin\varphi_x\cos\theta_{x,\mathrm{b}} & \hat{X}_{\mathrm{Mb}}\sin\varphi_x\sin\theta_{x,\mathrm{b}} & 0 \\ \hat{X}_{\mathrm{M}}\cos\theta_x & \hat{X}_{\mathrm{M}}\sin\theta_x & 0 \end{bmatrix}. \tag{39}$$

This expression clearly shows that the drive components of the voltage and the current ($\hat{X}_{\mathrm{M}}\cos\theta_x$ and $\hat{X}_{\mathrm{M}}\sin\theta_x$) are 'seen' as a zero component (x_{0d} and x_{0q}) for the rotary direction, which also corresponds to (31) where the drive component is the same in all rows of the matrix $\mathbf{X}_{\mathrm{abc}}$. Accordingly, also the 'abc' flux linkage $\mathbf{\Psi}_{\mathrm{abc}}$ is transformed into the 'dq0' flux linkage which results in

$$\mathbf{\Psi}_{\mathrm{dq0}} = \begin{bmatrix} x\chi_{\mathrm{pm,M}}\cos\theta_\psi & x\chi_{\mathrm{pm,M}}\sin\theta_\psi & 0 \\ y\chi_{\mathrm{pm,M}}\cos\theta_\psi & y\chi_{\mathrm{pm,M}}\sin\theta_\psi & 0 \\ \hat{\Psi}_{\mathrm{M}}\cos\theta_\psi & \hat{\Psi}_{\mathrm{M}}\sin\theta_\psi & 0 \end{bmatrix}. \tag{40}$$

The 'dq' frame is usually oriented such that $\theta_\psi = 0°$, which leads to only three nonzero flux linkage components

$$\mathbf{\Psi}_{\mathrm{dq0}} = \begin{bmatrix} x\chi_{\mathrm{pm,M}} & 0 & 0 \\ y\chi_{\mathrm{pm,M}} & 0 & 0 \\ \hat{\Psi}_{\mathrm{M}} & 0 & 0 \end{bmatrix}. \tag{41}$$

As already done in **Sec. II-G** for separate windings, in order to identify the 'dq0' current components that contribute to the radial forces (F_{x} and F_{y}) and the thrust force (F_{z}) generation in matrix notation for the combined winding, the electrical and mechanical powers are compared. The electrical power of the MALTA winding is $p_{\mathrm{el}} = \sum_{m=\{a,b,c\}}\sum_{n=\{A,B,C\}} u_{mn}i_{mn}$, which can be expressed by the Frobenius inner product [35] of matrices, i.e. the sum of the element by element multiplication, as

$$p_{\mathrm{el}} = \langle \mathbf{U}_{\mathrm{abc}}, \mathbf{I}_{\mathrm{abc}} \rangle_{\mathrm{F}}, \tag{42}$$

where the MALTA voltage $\mathbf{U}_{\mathrm{abc}}$ is given as

$$\mathbf{U}_{\mathrm{abc}} = \mathbf{R}_{\mathrm{abc}}\mathbf{I}_{\mathrm{abc}} + \mathbf{L}_{\mathrm{abc}}\frac{d\mathbf{I}_{\mathrm{abc}}}{dt} + \frac{d\mathbf{\Psi}_{\mathrm{abc}}}{dt}. \tag{43}$$

The resistance $\mathbf{R}_{\mathrm{abc}}$ and the inductance $\mathbf{L}_{\mathrm{abc}}$ matrices are diagonal matrices, i.e. $\mathbf{R}_{\mathrm{abc}} = \mathrm{diag}(R,R,R)$ and $\mathbf{L}_{\mathrm{abc}} = \mathrm{diag}(L,L,L)$. Hence, the electrical power is equal to

$$\begin{aligned} p_{\mathrm{el}} = &\frac{9}{4}\Bigg\{ R\hat{I}_{\mathrm{Mb}}^2 + L\frac{d\hat{I}_{\mathrm{Mb}}}{dt}\hat{I}_{\mathrm{Mb}} + \\ &\chi_{\mathrm{pm,M}}\left(v_{\mathrm{x}}i_{\mathrm{dd}} + v_{\mathrm{y}}i_{\mathrm{qd}}\right) + \omega_{\mathrm{L}}\chi_{\mathrm{pm,M}}(xi_{\mathrm{dq}} + yi_{\mathrm{qq}})\Bigg\} + \\ &\frac{9}{2}\Bigg\{ R\hat{I}_{\mathrm{M}}^2 + L\frac{d\hat{I}_{\mathrm{M}}}{dt}\hat{I}_{\mathrm{M}} + \frac{d\hat{\Psi}_{\mathrm{M}}}{dt}i_{\mathrm{0d}} + \omega_{\mathrm{L}}\hat{\Psi}_{\mathrm{M}}i_{\mathrm{0q}}\Bigg\}, \end{aligned} \tag{44}$$

where $d\chi_{\mathrm{pm,M}}/dt = 0$ is assumed. From (44), the power parts that contribute to the copper losses (contain R), change of the magnetic energy (contain L or $d\hat{\Psi}_{\mathrm{M}}/dt$) and the mechanical power (contain v_{x}, v_{y} or ω_{L}) can be easily identified. It should be noted that $\omega_{\mathrm{L}} = (2\pi/\tau_{\mathrm{pp}})\,v_{\mathrm{z}}$. On the other hand, the mechanical power of the MALTA is equal to $p_{\mathrm{mech}} = v_{\mathrm{x}}F_{\mathrm{x}} + v_{\mathrm{y}}F_{\mathrm{y}} + v_{\mathrm{z}}F_{\mathrm{z}}$. Therefore, the thrust force in the MALTA with the combined winding is generated as

$$F_{\mathrm{z}} = \frac{9\pi}{\tau_{\mathrm{pp}}}\hat{\Psi}_{\mathrm{M}}i_{\mathrm{0q}}, \tag{45}$$

while the bearing forces are generated as

$$F_{\mathrm{x}} = \frac{9}{4}\chi_{\mathrm{pm,M}}i_{\mathrm{dd}}, \qquad F_{\mathrm{y}} = \frac{9}{4}\chi_{\mathrm{pm,M}}i_{\mathrm{qd}}, \tag{46}$$

which agrees with the analysis conducted using the complex space vector (cf. (26) and (27)). Additionally, the parasitic thrust force is created when the rotor radial displacement is nonzero, which is equal to $F_{\mathrm{z,par}} = (9\pi/2\tau_{\mathrm{pp}})\,\hat{\Psi}_{\mathrm{M}}(xi_{\mathrm{dq}} + yi_{\mathrm{qq}})$ which has to be compensated by the controller.

B. MALTA Reduced Transformation

In a second step, now a transformation has to be found which transforms the 9 'dq0' quantities into only the 4 'dq0' quantities, which are needed to control the forces generated in the MALTA. From (45) and (46) it can be seen that the thrust force F_z and the bearing forces F_x and F_y are controlled with three different 'dq0' current components. The rest of the current components have to be kept to zero by the current controller. Hence, the $\mathbf{I}_\mathrm{dq0}$ has the following form

$$\mathbf{I}_\mathrm{dq0} = \begin{bmatrix} i_\mathrm{dd} \to F_\mathrm{x}/K_\mathrm{B} & i_\mathrm{dq} \to 0 & i_\mathrm{d0} \to 0 \\ i_\mathrm{qd} \to F_\mathrm{y}/K_\mathrm{B} & i_\mathrm{qq} \to 0 & i_\mathrm{q0} \to 0 \\ i_\mathrm{0d} \to 0 & i_\mathrm{0q} \to F_\mathrm{z}/K_\mathrm{L} & i_\mathrm{00} \to 0 \end{bmatrix}, \quad (47)$$

where $K_\mathrm{L} = (9\pi/\tau_\mathrm{pp})\,\hat{\Psi}_\mathrm{M}$ and $K_\mathrm{B} = (9/4)\,\chi_\mathrm{pm,M}$ are the MALTA drive and bearing constants (cf. (45) and (46)). It should be noted that by keeping the current components in (47) to zero, the electrical angles φ_x, θ_x and $\theta_{x,\mathrm{b}}$ of the phase currents have to be controlled. Comparing (47) and (39), it can be seen that when controlling $i_\mathrm{0d} \to 0$, the drive current phase angle $\theta_i = \pi/2$ is achieved and when controlling $i_\mathrm{dq} \to 0$ or $i_\mathrm{qq} \to 0$, the bearing current phase angle $\theta_{i,\mathrm{b}} = 0$ results. Finally, the phase angle φ_i is determined by the current components i_dd and i_qd ($i_\mathrm{dd} = \hat{I}_\mathrm{Mb}\cos\varphi_i$ and $i_\mathrm{qd} = \hat{I}_\mathrm{Mb}\sin\varphi_i$) as $\varphi_i = \mathrm{atan2}(i_\mathrm{qd}, i_\mathrm{dd})$, which can be also obtained as $\varphi_i = \mathrm{atan2}(F_\mathrm{y}, F_\mathrm{x})$ due to the proportionality between the currents i_qd, i_dd and F_y, F_x, respectively, (cf. (46)).

Since $\mathbf{I}_\mathrm{dq0}$ has nine current components, the control system of the MALTA would need nine independent current controllers per MALTA module (the complete MALTA system consists of two such independently controllable modules, since a possible tilting of the long MALTA rotor has to be counteracted). In order to reduce the number of the required current controllers, a reduced transformation that requires only four current controllers per MALTA module is proposed. Since there is no rotation in the MALTA ($\omega_\mathrm{R} = 0$), the three-phase system in the rotary direction resembles 'DC' quantity. Therefore, it is enough to control only its amplitude $\hat{I}_\mathrm{Mb}$, while the information about the phase and the electrical angle φ_i is given by the radial position controllers that output the bearing forces F_x and F_y. Hence, the angle φ_i is always pointing in the direction in which the bearing force has to act. The transformation that gives only 4 'dq' components is defined as

$$\mathbf{X}_\mathrm{dq} = \begin{bmatrix} \hat{X}_\mathrm{M}\cos\theta_x & \hat{X}_\mathrm{M}\sin\theta_x \\ \hat{X}_\mathrm{Mb}\cos\theta_{x,\mathrm{b}} & \hat{X}_\mathrm{Mb}\sin\theta_{x,\mathrm{b}} \end{bmatrix} = \mathbf{K}_\mathrm{R}(\varphi_x)\cdot\mathbf{X}_\mathrm{abc}\cdot\mathbf{K}_\mathrm{L}, \quad (48)$$

where the transformation matrices $\mathbf{K}_\mathrm{R}(\varphi_x)$ and $\mathbf{K}_\mathrm{L}$ are

$$\mathbf{K}_\mathrm{R}(\varphi_x) = \frac{2}{3}\begin{bmatrix} 1/2 & -\sin(\varphi_x - \pi/2 + \gamma_\mathrm{a}) \\ 1/2 & -\sin(\varphi_x - \pi/2 + \gamma_\mathrm{b}) \\ 1/2 & -\sin(\varphi_x - \pi/2 + \gamma_\mathrm{c}) \end{bmatrix}^\top, \quad (49)$$

and

$$\mathbf{K}_\mathrm{L} = \frac{2}{3}\begin{bmatrix} \cos(\omega_\mathrm{L}t + \gamma_\mathrm{a}) & -\sin(\omega_\mathrm{L}t + \gamma_\mathrm{a}) \\ \cos(\omega_\mathrm{L}t + \gamma_\mathrm{b}) & -\sin(\omega_\mathrm{L}t + \gamma_\mathrm{b}) \\ \cos(\omega_\mathrm{L}t + \gamma_\mathrm{c}) & -\sin(\omega_\mathrm{L}t + \gamma_\mathrm{c}) \end{bmatrix}. \quad (50)$$

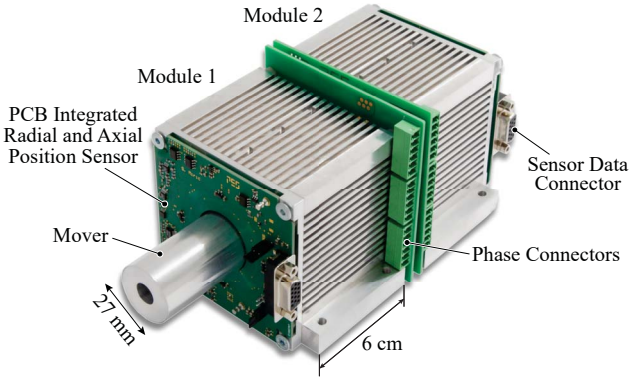

Fig. 7: The realized MALTA prototype. Each of the two modules (*Module 1* and *Module 2*) contain the 9-phase winding system as shown in **Fig. 6(a)**. The rotor realization is shown in **Fig. 6(b)**, where $\tau_\mathrm{pp} = 30\,\mathrm{mm}$.

Comparing the new 'dq' components in $\mathbf{X}_\mathrm{dq}$ given with (48) to the 'dq0' components in $\mathbf{X}_\mathrm{dq0}$ given with (39), it can be seen that the rotary zero sequence components x_0d and x_0q are moved to the first row of the $\mathbf{X}_\mathrm{dq}$. In the second row the components proportional to the bearing amplitude $\hat{X}_\mathrm{Mb}$ are found. In order not to generate any thrust force F_z with the bearing current component, the electrical angle $\theta_{i,\mathrm{b}} = 0$. Similarly, to maximize the thrust force generation with the drive current component $\hat{X}_\mathrm{M}$, the electrical angle $\theta_i = \pi/2$. In order to achieve these electrical angles, the components $\mathbf{X}_\mathrm{dq}(1,1)$ and $\mathbf{X}_\mathrm{dq}(2,2)$ are controlled to zero

$$\mathbf{I}_\mathrm{dq} = \begin{bmatrix} i_\mathrm{0d} \to 0 & i_\mathrm{0q} \to F_\mathrm{z}/K_\mathrm{L} \\ i_\mathrm{bd} \to F_\mathrm{B}/K_\mathrm{B} & i_\mathrm{bq} \to 0 \end{bmatrix}, \quad (51)$$

where $i_\mathrm{bd} = \hat{I}_\mathrm{Mb}\cos\theta_{x,\mathrm{b}}$, $i_\mathrm{bq} = \hat{I}_\mathrm{Mb}\sin\theta_{x,\mathrm{b}}$ and $F_\mathrm{B} = \sqrt{F_\mathrm{x}^2 + F_\mathrm{y}^2}$. The force angle $\varphi_i = \mathrm{atan2}(F_\mathrm{y}/F_\mathrm{x})$ is calculated from the bearing force references F_x and F_y, which are provided from the radial position controller as shown in the following section.

IV. MALTA System Implementation

In order to verify the complex space vector modeling approach conducted in **Sec. III** on the basis of a MALTA with combined windings, the MALTA prototype and the corresponding power electronic inverter drive are implemented in hardware. In the following, each part of the magnetically levitated linear motor drive system is described.

A. MALTA Prototype

The implemented MALTA prototype is shown in **Fig. 7**. In order to be able to also control the tilting of the long MALTA rotor, the prototype consists of two modules, i.e. *Module 1* and *Module 2*, where each of the modules has 9-phase windings as shown in **Fig. 6(a)** and can generate thrust and bearing forces. Therefore, the implemented prototype has 18-phases in total. It should be noted that the number of the MALTA modules may be arbitrary, but must be larger than two.

The rotor of the MALTA is realized with axially magnetized PM rings, stacked together with iron rings as shown in

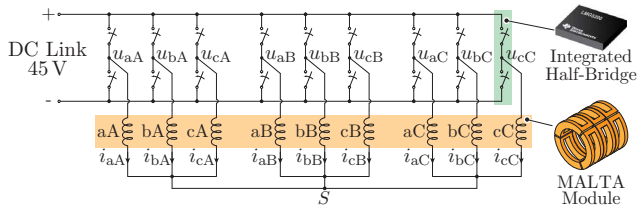

Fig. 8: Circuit diagram of the 9-phase MALTA module drive system. The two-level inverter is implemented with galium nitride (GaN) half-bridges (*Texas Instruments LMG5200*).

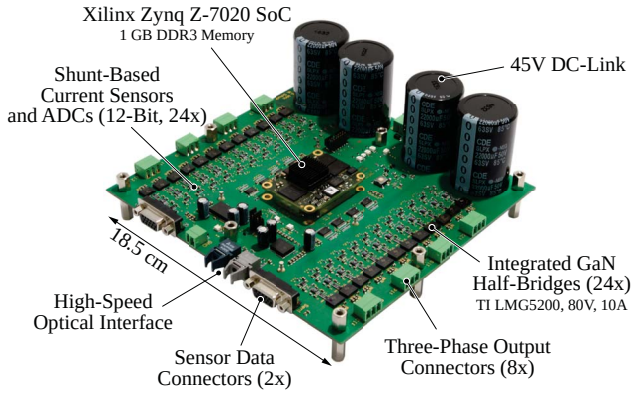

Fig. 9: Two-level MALTA inverter that consists of 24 chip integrated half-bridges, control board and digital interfaces for position sensors.

Fig. 6(b). With this realization, the iron rings create the PM poles that magnetically interact with the MALTA winding. The rotor is covered with a $0.3\,\mathrm{mm}$ thick aluminum shield, which on the one hand provides a mechanical protection of the rotor PMs and on the other hand is used as a conductive surface for the radial, eddy-current based, position sensor, [32]. For the axial position measurement, Hall-effect sensors are used, which measure the PM axial field component.

More details about the MALTA design and measurements can be found in [16].

B. MALTA Power Electronic Inverter Drive

The electrical schematic of a single MALTA module is shown in **Fig. 8**.

The power electronics inverter is realized as a 24-phase two-level converter that can drive all windings of two MALTA modules, while on the other side the windings of each module are connected to a single star point S. A picture of the hardware of the inverter employing 24 chip integrated half-bridges and a high-performance control board (*Xilinx Zynq Z-7020 SoC*) is shown in **Fig. 9**. In each control interrupt routine, in total 30 measurement signals (24 current measurements and 6 signals from the position sensors) are collected in parallel with 12-bit external ADCs.

C. MALTA Control Algorithm

The MALTA control block diagram is shown in **Fig. 10**. A cascaded control structure can be recognized, with inner (faster) current control loop and outer (slower) position control loop. For each control variable, an individual single-input single-output (SISO) controller is used. Therefore, in total 8 current controllers (4 per module) and 5 position controllers (4 for radial and 1 for axial positions) are needed.

The outer position controllers are realized as Proportional-Integral-Derivative (PID) controllers which translate the position error $\vec{r}^{*} - \vec{r}$ at the controller input into a corresponding force $\vec{F}_{\mathrm{c}}$ at the controller output. In particular, the radial positions $x^{(1,2)}, y^{(1,2)}$ sensed at each module are controlled with the corresponding bearing forces $F_{\mathrm{x}}^{(1,2)}, F_{\mathrm{y}}^{(1,2)}$ generated by the same module. It should be pointed out that derivative action is needed in order to stabilize the mechanical system, as it shows second order double integrator dynamics. Furthermore, this is implemented with a relocation on the feedback path, i.e. it is computed directly from the output r rather than the control error $\vec{r}^{*} - \vec{r}$. This allows suppressing a zero in the resulting closed loop transfer function, as it can be verified analytically, with the advantage of reducing overshoot and ringing in the response.

Based on the bearing and thrust force constants

$$K_{\mathrm{B}} = \frac{9}{4}\chi_{\mathrm{pm,M}}, \qquad K_{\mathrm{L}} = \frac{9\pi}{\tau_{\mathrm{pp}}}\hat{\Psi}_{\mathrm{M}} \tag{52}$$

the force commands are then converted into the corresponding desired 'dq' current commands $\mathbf{I}_{\mathrm{dq}}^{*(1,2)}$, which are the setpoints for the inner current controllers. The advantage of the complex space vector model of the MALTA presented in **Sec. II-G** is now apparent, as it allows controlling a highly sophisticated multi-phase machine with established control techniques. In fact, each transformed 'dq' current component evolves then like a first order RL network, which can be regulated with a simple Proportional-Integral (PI) control. Moreover, with a minimal number of only four controlled quantities, it is possible at any moment in time to assign all of the nine phase voltages.

The measured axial position z is used to compute the linear electrical angle for the 'dq' transformation. Additionally, it is used for the feed-forward action $\vec{F}_{\mathrm{ff}}(z)$ by the position controller, which compensates for the gravity and other detent forces such as cogging force and the radial pull force. The function $\vec{F}_{\mathrm{ff}}(z)$ is experimentally recorded using the position controller reference signal in steady-state.

Due to the cascaded control structure, the bandwidth specification for the current controllers can be directly derived from the desired performances of the outer position control loop. The requirements for radial and axial position control are slightly different and are discussed separately in the following.

The needed dynamics of the radial position are determined for $x^{(1,2)}$ and $y^{(1,2)}$ directions and are the same for both modules (*Module 1* and *Module 2*, (cf. **Fig. 7**)). Therefore, in the following the module notation is omitted and only x and y are used.

Furthermore, it is assumed that the radial subsystems of *Module 1* and *Module 2* are totally independent and each module is suspending one half of the rotor mass. If it is further assumed that the $x-$ and $y-$direction are completely

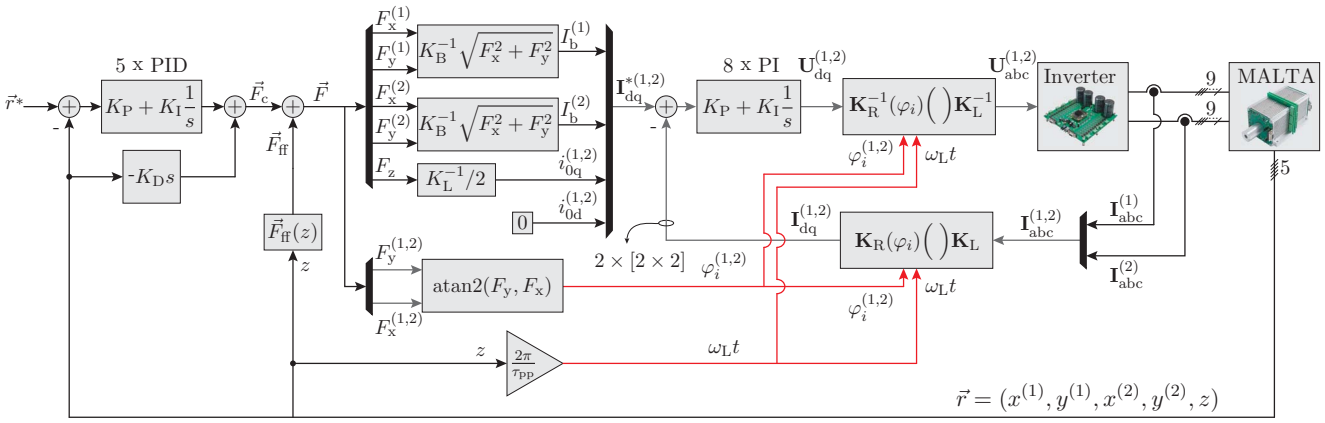

Fig. 10: Cascaded MALTA position controller structure with the outer position controller loop and the inner current controller loop. In total 5 positions (4 radial and 1 axial) are independently controlled with the separate 5 PID controllers. All of them have the same gains that are given in **Tab. II** in the Appendix. The electrical angles $\varphi_i^{(1,2)}$ and $\omega_{\mathrm{L}}t$ needed for the reduced transformation are shown with red arrows. In the feed-forward path, the steady-state disturbances (such as gravity and the radial pull forces caused by the manufacturing tolerances) are compensated when the rotor is in the center. By adding the force reference from the controller $\vec{F}_{\mathrm{c}}$ and the feed-forward force reference $\vec{F}_{\mathrm{ff}}(z)$, the total force reference vector $\vec{F} = \vec{F}_{\mathrm{c}} + \vec{F}_{\mathrm{ff}}(z) = (F_{\mathrm{x}}^{(1)}, F_{\mathrm{y}}^{(1)}, F_{\mathrm{x}}^{(2)}, F_{\mathrm{y}}^{(2)}, F_{\mathrm{z}})$ is created. The components of $\vec{F}$ are used to form the current controller references and to calculate the radial force angles $\varphi_i^{(1,2)}$ required for the rotary transformation matrix $\mathbf{K}_{\mathrm{R}}(\varphi_i)$ and its inverse $\mathbf{K}_{\mathrm{R}}^{-1}(\varphi_i)$ (cf. Appendix). For the current control loop, 9 'abc' phase currents are measured per MALTA module and transformed into the 'dq' frame using the reduced MALTA transformation, (cf. **Sec. III-B**). In total, $2 \times 4 = 8$ PI current controllers are implemented and tuned according to **Tab. II**.

decoupled, the accelerations are obtained as

$$a_{\mathrm{x}} = \frac{2}{m} F_{\mathrm{x}}, \qquad a_{\mathrm{y}} = \frac{2}{m} F_{\mathrm{y}} \tag{53}$$

where $a_{\mathrm{x}} = d^2x/dt^2$ and $a_{\mathrm{y}} = d^2y/dt^2$ are the radial accelerations and m is the rotor mass. In (53) the half mass is accelerated as each of the modules lifts only a half of the rotor, cf. **Fig. 7**. In the Laplace domain, the open loop transfer function of the plant representing the radial positions is equal to

$$G_{\mathrm{OL}}(s) = \frac{\{x(s), y(s)\}}{F_{\{\mathrm{x,y}\}}(s)} = \frac{2}{m\, s^2}, \tag{54}$$

where $s = \mathcal{L}(d/dt)$ is the Laplace transform of the time derivative. The desired radial position is zero at all times, i.e. the rotor is located in the center of the stator. Hence, the main specification for x and y can be expressed in terms of rejection of the external mechanical disturbing forces (gravity force and the radial pull force) that deviate the rotor from its center position. The most relevant are the radial pull forces $F_{\mathrm{x,pull}}$, $F_{\mathrm{y,pull}}$ between the rotor PMs and the stator. These destabilizing radial pull forces are measured to be linearly proportional within the possible mechanical air gap (small signal) to the radial displacement according to the radial pull constant K_{pull}

$$F_{\mathrm{pull,x}} = x\, K_{\mathrm{pull}}, \qquad F_{\mathrm{pull,y}} = y\, K_{\mathrm{pull}} \tag{55}$$

and represent an input disturbance for the radial subsystems (53). The value of the radial pull constant for the MALTA is measured to be $K_{\mathrm{pull}} = 8330\,\mathrm{N\,m^{-1}}$ [16].

In a classic feedback control, the closed loop bandwidth requirement of the control system may be imposed by the disturbances as [36]

$$\omega_{\mathrm{BW}} > \omega_{\mathrm{D}}, \qquad \omega_{\mathrm{D}} \text{ such that } \|G_{\mathrm{D}}^{\mathrm{pu}}(j\omega_{\mathrm{D}})\| = 1 \tag{56}$$

where ω_{BW} is the required closed loop bandwidth and $G_{\mathrm{D}}^{\mathrm{pu}}$ is the open loop disturbance transfer function in per units (unit-magnitude scaled). Since the disturbance is the radial pull force, the open loop disturbance transfer function is equal to the radial position plant (54), i.e. $G_{\mathrm{D}} = G_{\mathrm{OL}}$. As the requirement (56) is applied in per unit system, the transfer function G_{D} should be normalized. For example, for the x radial direction the G_{D} is normalized using the maximum expected displacements $\hat{x}$ and the pull force $\hat{F}_{\mathrm{pull,x}}$ as

$$G_{\mathrm{D}}^{\mathrm{pu}}(s) = \frac{x(s)/\hat{x}}{F_{\mathrm{x}}(s)/\hat{F}_{\mathrm{x}}} = \frac{2K_{\mathrm{pull}}}{m\, s^2}, \tag{57}$$

where $\hat{F}_{\mathrm{x}} = \hat{x}\, K_{\mathrm{pull}}$. Using (56), the angular frequency ω_{D} is calculated as $\omega_{\mathrm{D}} = \sqrt{2K_{\mathrm{pull}}/m}$. Therefore, the closed loop bandwidth of the radial position controller should be bigger then

$$\omega_{\mathrm{BW}} > \sqrt{\frac{2\, K_{\mathrm{pull}}}{m}} \approx 220\,\mathrm{rad\,s^{-1}}, \tag{58}$$

where the values for K_{pull} and m are given in the Appendix in **Tab. I**. The same applies analogously for the radial subsystem in $y-$direction.

In order to guarantee the appropriate dynamic decoupling between the inner and outer control loops, the current control bandwidth has to be at least 5 times higher than the outer position controller bandwidth ω_{BW}, i.e. at least $1100\,\mathrm{rad\,s^{-1}}$.

The axial position z evolves similarly according to the axial subsystem dynamics $a_{\mathrm{z}} = F_{\mathrm{z}}/m$, where $a_{\mathrm{z}} = d^2z/dt^2$ is the axial acceleration and m is the mass of the MALTA rotor. The specifications for z depend on the desired dynamics and are usually specified in the time domain for a step response, mainly in terms of the desired rise time t_{r}. In order to tune the inner current controller loop, the closed loop bandwidth

should be given, which can be related to the rise time as $f_{\mathrm{BW}}\, t_{\mathrm{r}} = 1/3$ [37], where $f_{\mathrm{BW}} = \omega_{\mathrm{BW}}/2\pi$. Typical rise times of tubular linear motors with similar size are in the range of $t_{\mathrm{r}} = 20\,\mathrm{ms}$ [38]. Therefore, to achieve this rise time, the closed loop bandwidth of the axial position controller should be bigger then $\approx 110\,\mathrm{rad\,s^{-1}}$, which is half of the requirement for the radial position controller that has to suppress the radial pull disturbances (cf. (58)).

Finally, in order to achieve a proper dynamic decoupling from the position controller, the current controllers are tuned to a bandwidth of $3000\,\mathrm{rad\,s^{-1}}$, which gives some margin to allow for faster position controller designs and it is useful to suppress radial and axial deviations even under stronger external disturbances. In fact, for this purpose, the final bandwidth of the radial position controllers is chosen to be around two times larger than the minimum required bandwidth ω_{BW} in (58), i.e. $\omega_{\mathrm{BW}} \approx 400\,\mathrm{rad\,s^{-1}}$.

The corresponding position and current control PID gains are listed in **Tab. II** in the Appendix.

V. Measurements and Results

In this section the implemented control algorithm is verified with experimental measurements. All the signals are measured with internal sensors, collected by the firmware and transmitted to a user interface after the experiment is concluded. The following expermiments are performed: (1) the system is started and stable levitation of the rotor is achieved (cf. **Fig. 11**); (2) linear motor operation is performed by giving a sinusoidal reference along the axial direction (cf. **Fig. 13**). The measurements show stable levitation and successful decoupling of the bearing and thrust force control.

A. Soft Start-Up

Initially, the MALTA rotor is located in its rest position on the touch-down bearing ($x_0^{(1)} = 0.1\,\mathrm{mm}$, $y_0^{(1)} = -0.7\,\mathrm{mm}$, $z_0 = -1\,\mathrm{mm}$). In order to avoid abrupt controller responses and provide a smooth lift up instead, the reference is shaped to guide the rotor from its start position to the center of the machine ($x^{(1)*} = 0$, $y^{(1)*} = 0$) as shown in **Fig. 11(c)**. The selected reference is a filtered step with a cutoff frequency of $\approx 67\,\mathrm{rad\,s^{-1}}$, i.e. the step response of the first order system

$$R(s) = \frac{1}{0.015\,s + 1} \tag{59}$$

discretized at the sampling time $T_{\mathrm{s}} = 50\,\mu\mathrm{s}$, which reaches the final value in $0.1\,\mathrm{s}$. This is then appropriately scaled to reach the zero position starting from the initial $x_0^{(1)}$ and $y_0^{(1)}$ positions as

$$x^{(1)*} = x_0^{(1)}\,(1 - r(t)) \tag{60}$$

$$y^{(1)*} = y_0^{(1)}\,(1 - r(t)) \tag{61}$$

where $r(t) = \mathcal{L}^{-1}\,(R(s)/s)$ is the step response of (59) and $\mathcal{L}^{-1}$ the inverse Laplace transform operator. The positions $x_0^{(1)}$ and $y_0^{(1)}$ are measured during an offset calibration routine executed once before the regular machine operation is started.

In order to overcome pull and gravity forces $F_{\mathrm{pull,y}}^{(1)}$ and $F_{\mathrm{g}} = g\,m/2 = 3.53\,\mathrm{N}$, with $g = 9.8\,\mathrm{m\,s^{-2}}$ the gravity

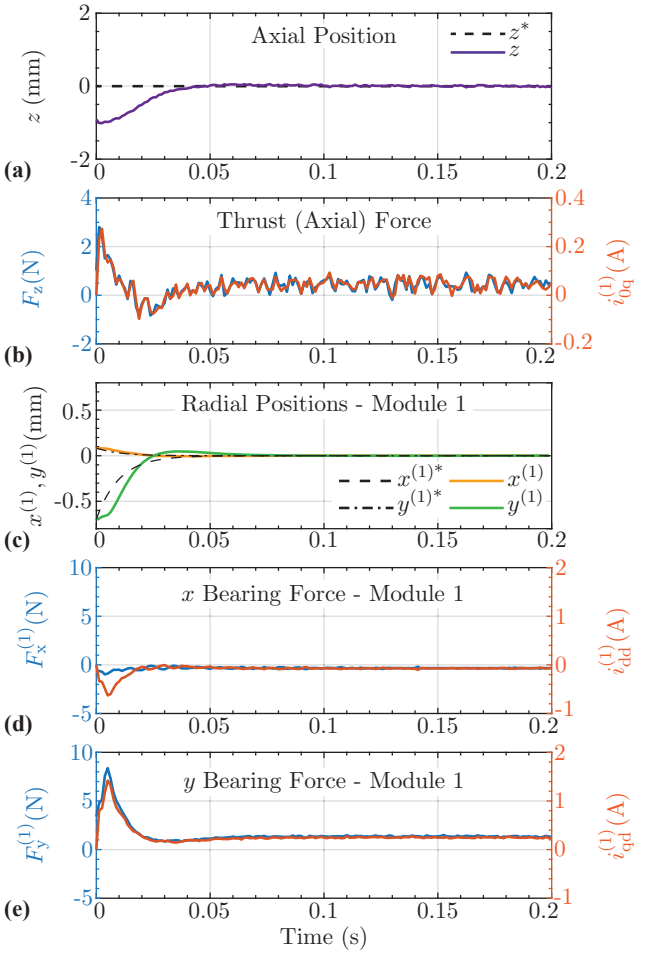

Fig. 11: Measurements of the MALTA start-up experiment where the rotor in its initial position touches the touch down bearing ($x_0^{(1)} = 0.1\,\mathrm{mm}$, $y_0^{(1)} = -0.7\,\mathrm{mm}$ and $z_0 = -1\,\mathrm{mm}$) and lifts up to the reference value ($x^{(1)*} = 0$, $y^{(1)*} = 0$ and $z^* = 0$). Radial positions of the first module ($x^{(1)}, y^{(1)}$) and the axial position (z) are shown. The shown force components are denoted in the control block diagram shown in **Fig. 10**. The current 'dq0' components (cf. (47)) responsible for the respective force components are labeled on the right side of the plots.

acceleration, the integral part of the controller starts increasing the commanded $F_{\mathrm{y}}^{(1)}$ (cf. **Fig. 11(e)**). As soon as the balance condition

$$F_{\mathrm{y}}^{(1)} = F_{\mathrm{pull,y}}^{(1)} + F_{\mathrm{g}} \approx 8.3\,\mathrm{N} \tag{62}$$

is reached, the rotor lifts up. This happens at $0.005\,\mathrm{s}$, when the current component $i_{\mathrm{qd}}^{(1)}$ reaches the value $1.42\,\mathrm{A}$, producing the bearing force $F_{\mathrm{y}}^{(1)} = K_{\mathrm{B}}\, i_{\mathrm{qd}}^{(1)} \approx 8.3\,\mathrm{N}$, which verifies the derived bearing constant.

The rotor then approaches the center of the machine with small overshoots (below $10\,\%$) both in x and y directions and finally reaches steady state at around $0.06\,\mathrm{s}$, with an error which remains confined within $\pm 1\,\mu\mathrm{m}$.

Simultaneously, also the axial position z reaches the zero setpoint, with a steady state error of $\pm 20\,\mu\mathrm{m}$. The larger deviation in axial direction comes from the higher amount of

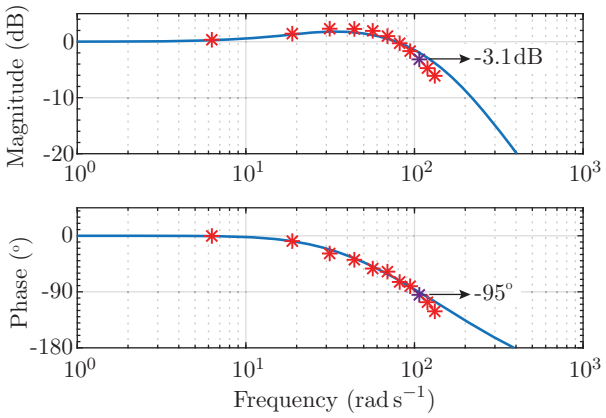

Fig. 12: Experimental verification of the Bode magnitude and phase diagrams for the closed loop axial subplant of MALTA. The solid blue line corresponds to the predicted, analytically derived closed loop transfer function, whereas the red stars represent experimental measurements at the corresponding frequencies $f_z = \{1, 3, 5, \ldots, 19, 21\}$Hz, i.e. regular intervals of 2 Hz from 1 up to 21 Hz. The 17 Hz experiment is shown in time in **Fig. 13** (the measurement highlighted in violet).

the axial sensor noise, which is due to the chosen Hall effect sensing method.

Moreover, in **Fig. 11(b)** one can observe that F_z and the corresponding current component $i_{0q}^{(1)}$ show a non-zero average value of $\approx 0.5\,\mathrm{N}$ and $\approx 0.05\,\mathrm{A}$ respectively, which are needed in order to compensate the cogging force and to maintain the rotor in the desired axial position. It should be noted that the plotted F_z is the overall thrust force, i.e. the sum of the individual forces produced by the two modules, whereas $i_{0q}^{(1)}$ is the corresponding current component only of the first module.

B. Linear Motor Operation

The linear motor operation is tested and verified with a periodic sinusoidal axial movement, where mass of the mover serves as a load. This kind of experiment is well justified for applications such as pick-and-place robot in semiconductor/electronics industry. In such cases, the mass of the moved and placed components is much smaller then the mass of the mover. In **Fig. 12**, the Bode magnitude and phase diagrams for the closed loop axial subplant are shown. These are derived analytically from the simplified axial model and by using the PID gains of **Tab. II**. Furthermore, they are experimentally validated with axial positions measurements for different frequencies of the sinusoidal reference, and the computed magnitudes and phases are reported on the diagram. In particular, f_z is chosen at regular intervals of 2 Hz from 1 up to 21 Hz. As it can be observed, predicted and measured frequency responses are in good agreement and the mismatches appearing after $100\,\mathrm{rad\,s^{-1}}$ can be justified with the neglected eddy current breaking effects and other nonlinearities.

The controlled axial system is capable of tracking sinusoidal references up to $10\,\mathrm{rad\,s^{-1}}$, whereas faster signals would experience some amplification, which is however below 2 dB. After around $100\,\mathrm{rad\,s^{-1}}$, the gain of the system starts rolling off with -40 dB/dec slope. Concerning the phase shift

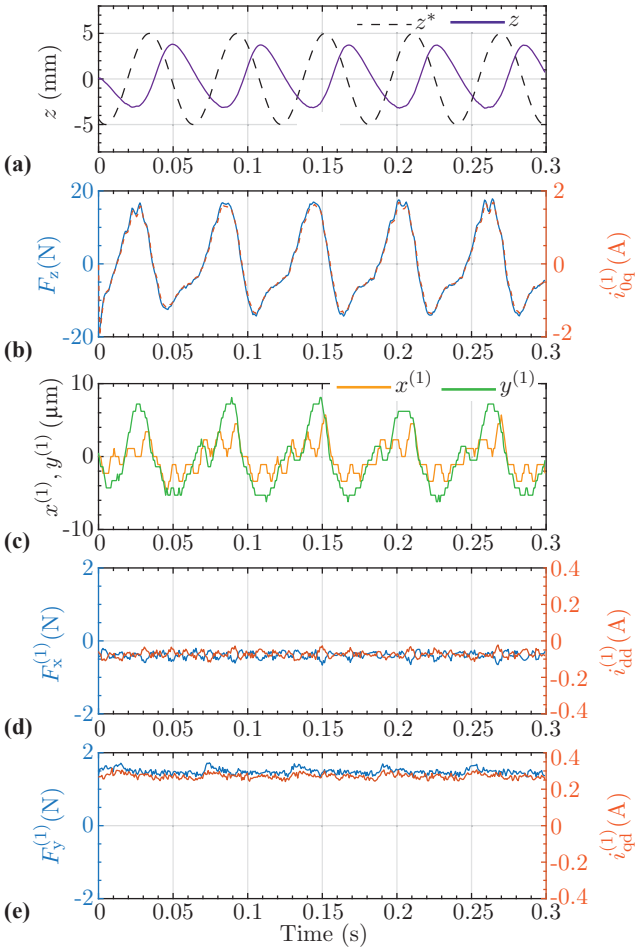

Fig. 13: Measurements of the MALTA linear motor operation, where a sinusoidal reference for the axial position is given $z^* = 5\,\mathrm{mm}\cos(2\pi\,17\,\mathrm{Hz})$. The response is attenuated by 0.707 (-3 dB) as the closed loop axial position controller bandwidth is tuned to 17 Hz. The radial position is slightly disturbed during the axial movements of the rotor and stays between $\pm 8\,\mu\mathrm{m}$. The radial forces are nonzero such that radial pull onto the rotor is compensated during the linear motor operation.

between reference and measured signals, this reaches $-90°$ for frequencies at around $100\,\mathrm{rad\,s^{-1}}$ and keeps decreasing towards $-180°$.

Therefore, the frequency of $f_z = 17\,\mathrm{Hz} \approx 107\,\mathrm{rad\,s^{-1}}$ for motor operation is chosen to verify the bandwidth of the axial control system. In fact, in **Fig. 13(a)** it can be observed that the amplitude of the measured axial position signal is reduced by -3 dB with respect to the original $\Delta z^*_{\mathrm{pp}} = 10\,\mathrm{mm}$ peak-to-peak amplitude, resulting in $\Delta z_{\mathrm{pp}} = 7\,\mathrm{mm}$. Additionally, as also expected a phase shift of $\phi \approx 95°$ is observed (cf. **Fig. 13(a)**).

The commanded F_z in **Fig. 13(b)** oscillates accordingly with $\Delta F_{z,\mathrm{pp}} = 29.26\,\mathrm{N}$ to provide the required acceleration.

Meanwhile, the radial positions oscillate slightly around their steady state position, but remain limited within $\pm 8\,\mu\mathrm{m}$ error thanks to the fast radial control tuning.

The corresponding bearing forces keep the rotor levitated while reacting against the disturbances from the fast axial

motion. In particular, the average value of $F_{\mathrm{y}}^{(1)}$ is $1.6\,\mathrm{N}$, which corresponds to the force required to balance the gravity force F_{g}. Concerning $F_{\mathrm{x}}^{(1)}$, an average value of $-0.37\,\mathrm{N}$ instead of the ideal zero can be observed. This is due to the radial pull force created by manufacturing tolerances of the real prototype.

VI. Conclusion

This paper focuses on the complex space vector modeling of electric machines with permanent magnet (PM) rotor covering all possible movements such as rotary, linear and radial, i.e. magnetic bearing (MB). To the authors best knowledge, for the first time in literature a complex space vector model of the rotary-linear machine with MBs is formulated, allowing to apply known complex space vector techniques used for years for modeling of electric machines. For example, the phase winding of the rotary-linear machine with 9 phases in total may be described with a single complex space vector voltage equation using the proposed transformation, which has the same form as the complex space vector voltage equation of the conventional rotary or linear machine. The torque, the thrust force and the radial (bearing) forces onto the rotor can be easily calculated using the proposed complex space vector model, which is of interest for understanding the machine operation and implementing the control system. In order to verify the complex space vector models, a control system for the linear actuator with MBs (so called MALTA) is successfully implemented and tested. As the MALTA has combined winding (the same winding is used for the bearing and thrust force generation), the components of the proposed complex space vector are written in matrix form and further analyzed. As shown in the paper, the quantities (voltage, current or flux linkage) for the thrust force generation are zero-sequence components in rotary direction for the bearing force quantities. The MALTA combined winding in stationary frame ('dq0' frame) is represented with 9 different components clarified in the paper. This would require 9 different current controllers to be implemented, which was the motivation to propose a reduced transformation that requires only 4 current controllers for its implementation. The discussed models that decouple the bearing force control and the thrust force control are verified by measurements. Two different measurement experiments are shown, start-up and linear motor operation. In the start-up experiment, the rotor of the MALTA is successfully lifted from rest to its center position. In the linear motor operation, the MALTA axial position is varied with a sinusoidal reference with a stroke of $10\,\mathrm{mm}$ and a mechanical frequency of $17\,\mathrm{Hz}$. During this operation mode, the radial position deviation stayed below $\pm 8\,\mu\mathrm{m}$. These results verify the proposed models and the position controller design.

The future work focuses on the implementation of the feed-forward position controller, deeper analysis of the mechanical model of the rotor and MIMO-LQR position controller development, which should allow to perform high-dynamic high-precision positioning tasks.

Appendix

MALTA Motor Parameters

The MALTA motor parameters are given in **Tab. I**.

TABLE I: MALTA Motor Parameters.

Symbol	Quantity	Value
Electrical		
R	phase winding resistance	$2.2\,\Omega$
L	phase winding inductance	$2.0\,\mathrm{mH}$
Mechanical		
m	mover mass	$0.360\,\mathrm{kg}$
Force Constants		
K_{L}	drive constant per module	$5.2\,\mathrm{N\,A^{-1}}$
K_{B}	bearing constant per module	$5.2\,\mathrm{N\,A^{-1}}$
K_{pull}	radial pull constant per module	$8330\,\mathrm{N\,m^{-1}}$

MALTA Controller Parameters

The MALTA controller parameters are given in **Tab. II**.

TABLE II: Position and current controller gains.

Variable	K_{P}	K_{I}	K_{D}
$i_{0\mathrm{q}}, i_{\mathrm{bd}}$	$8.01\,\mathrm{V\,A^{-1}}$	$8.45\,\mathrm{kV\,A^{-1}\,s^{-1}}$	-
$i_{0\mathrm{d}}, i_{\mathrm{bq}}$	$8.01\,\mathrm{V\,A^{-1}}$	$8.45\,\mathrm{kV\,A^{-1}\,s^{-1}}$	-
$x^{(1)}, x^{(2)}$	$39\,\mathrm{kN\,m^{-1}}$	$1.8\,\mathrm{MN\,m^{-1}\,s^{-1}}$	$150\,\mathrm{N\,s\,m^{-1}}$
$y^{(1)}, y^{(2)}$	$39\,\mathrm{kN\,m^{-1}}$	$1.8\,\mathrm{MN\,m^{-1}\,s^{-1}}$	$150\,\mathrm{N\,s\,m^{-1}}$
z	$2.44\,\mathrm{kN\,m^{-1}}$	$42.87\,\mathrm{kN\,m^{-1}\,s^{-1}}$	$35.07\,\mathrm{N\,s\,m^{-1}}$

Inverse MALTA Reduced Transformation

The inverse transformation matrices used in the control system from **Fig. 10** are equal to

$$\mathbf{K}_{\mathrm{R}}^{-1}(\varphi_x) = \begin{bmatrix} 1 & -\sin(\varphi_x - \pi/2 + \gamma_{\mathrm{a}}) \\ 1 & -\sin(\varphi_x - \pi/2 + \gamma_{\mathrm{b}}) \\ 1 & -\sin(\varphi_x - \pi/2 + \gamma_{\mathrm{c}}) \end{bmatrix}, \tag{63}$$

and

$$\mathbf{K}_{\mathrm{L}}^{-1} = \begin{bmatrix} \cos(\omega_{\mathrm{L}} t + \gamma_{\mathrm{a}}) & -\sin(\omega_{\mathrm{L}} t + \gamma_{\mathrm{a}}) \\ \cos(\omega_{\mathrm{L}} t + \gamma_{\mathrm{b}}) & -\sin(\omega_{\mathrm{L}} t + \gamma_{\mathrm{b}}) \\ \cos(\omega_{\mathrm{L}} t + \gamma_{\mathrm{c}}) & -\sin(\omega_{\mathrm{L}} t + \gamma_{\mathrm{c}}) \end{bmatrix}^{\top}. \tag{64}$$

References

[1] E. Lomonova, "Advanced Actuation Systems-State of the Art: Fundamental and Applied Research," in *Proc. of IEEE International Conference on Electrical Machines and Systems*, 2011, pp. 336–341.
[2] T. Overboom, J. Jansen, E. Lomonova, and F. Tacken, "Design and Optimization of a Rotary Actuator for a Two-Degree-of-Freedom $z-\varphi$ Module," *IEEE Trans. Ind. Appl.*, vol. 46, no. 6, pp. 2401–2409, 2010.
[3] K. J. Meessen, J. J. Paulides, and E. A. Lomonova, "Modeling and Experimental Verification of a Tubular Actuator for 20g Acceleration in a Pick-and-Place Application," *IEEE Trans. Ind. Appl.*, vol. 46, no. 5, pp. 1891–1898, 2010.
[4] P. R. Eckert, A. F. Flores Filho, E. Perondi, and D. G. Dorrell, "Dual Quasi-Halbach Linear Tubular Actuator with Coreless Moving-Coil for Semi-Active and Active Suspension," *IEEE Trans. Ind. Electron.*, 2018.
[5] X. Xue, K. W. E. E. Cheng, and Z. Zhang, "Model, Analysis and Application of Tubular Linear Switched Reluctance Actuator for Linear Compressors," *IEEE Trans. Ind. Electron.*, 2018.
[6] V. DelliColli, P. Cancelliere, F. Marignetti, R. DiStefano, and M. Scarano, "A Tubular-Generator Drive for Wave Energy Conversion," *IEEE Trans. Ind. Electron.*, vol. 53, no. 4, pp. 1152–1159, 2006.

[7] J. J. Paulides, J. L. Janssen, and E. A. Lomonova, "Bearing Lifetime of Linear PM Machines," in *Proc. of IEEE Energy Conversion Congress and Exposition (ECCE USA)*, 2009, pp. 1083–1090.
[8] K. Meessen, J. Paulides, and E. Lomonova, "Analysis and Design Considerations of a 2-DoF Rotary-Linear Actuator," in *Proc. of IEEE International Electric Machines & Drives Conference (IEMDC)*, 2011, pp. 336–341.
[9] K. J. Meessen, "Electromagnetic Fields and Interactions in 3D Cylindrical Structures: Modeling and Application," *Dept. Electric Eng., Eindhoven Univ. Technol., the Netherlands*, 2012.
[10] H. Bleuler, M. Cole, P. Keogh, R. Larsonneur, E. Maslen, Y. Okada, G. Schweitzer, A. Traxler *et al.*, *Magnetic Bearings: Theory, Design, and Application to Rotating Machinery*. Springer Science & Business Media, 2009.
[11] D. Steinert, T. Nussbaumer, and J. W. Kolar, "Slotless Bearingless Disk Drive for High-Speed and High-Purity Applications," *IEEE Tran. on Industrial Electronics*, vol. 61, no. 11, pp. 5974–5986, 2014.
[12] P. Puentener, M. Schuck, D. Steinert, T. Nussbaumer, and J. W. Kolar, "A 150 000-r/min Bearingless Slice Motor," *IEEE/ASME Tran. on Mechatronics*, vol. 23, no. 6, pp. 2963–2967, Dec 2018.
[13] M. Schuck, D. Steinert, T. Nussbaumer, and J. W. Kolar, "Ultrafast Rotation of Magnetically Levitated Macroscopic Steel Spheres," *Science Advances*, vol. 4, no. 1, p. e1701519, 2018.
[14] A. G. Rainer Gloess, "Nanometer Resolution of Magnetic Levitation Stages for Planar and Linear Scan Application," in *Proc. of International Symposium on Magnetic Bearings, ISMB*. source: magneticbearings.org, 2018, pp. 1–6.
[15] N.-C. Tsai and C.-W. Chiang, "Design and Analysis of Magnetically-Drive Actuator Applied for Linear Compressor," *Mechatronics*, vol. 20, no. 5, pp. 596–603, 2010.
[16] S. Mirić, P. Küttel, A. Tüysüz, and J. W. Kolar, "Design and Experimental Analysis of a New Magnetically Levitated Tubular Linear Actuator," *IEEE Tran. on Industrial Electronics*, vol. 66, no. 6, pp. 4816–4825, 2019.
[17] P. Jin, H. Lin, S. Fang, and S. Ho, "Decoupling Control of Linear and Rotary Permanent Magnet Actuator Using Two-Directional $d-q$ Transformation," *IEEE Trans. on Magnetics*, vol. 48, no. 10, pp. 2585–2591, 2012.
[18] H. B. Ertan, M. Y. Üçtug, R. Colyer, and A. Consoli, *Modern electrical drives*. Springer Science & Business Media, 2013, vol. 369.
[19] J. Pyrhonen, V. Hrabovcova, and R. S. Semken, *Electrical machine drives control: An introduction*. John Wiley & Sons, 2016.
[20] K. P. Kovács and I. Rácz, *Transiente vorgänge in Wechselstrommaschinen*. Verlag der ungarischen Akademie der Wissenschaften, 1959, vol. 1.
[21] A. Mora, R. Cárdenas, M. Espinoza, and M. Díaz, "Active Power Oscillation Elimination in 4-Leg Grid-Connected Converters Under Unbalanced Network Conditions," in *Proc. of Annual Conference of the IEEE Industrial Electronics Society (IECON)*, 2016, pp. 2229–2234.
[22] G. Sala, G. Valente, A. Formentini, L. Papini, D. Gerada, P. Zanchetta, A. Tani, and C. Gerada, "Space Vectors and Pseudoinverse Matrix Methods for the Radial Force Control in Bearingless Multisector Permanent Magnet Machines," *IEEE Tran. on Industrial Electronics*, vol. 65, no. 9, pp. 6912–6922, 2018.
[23] G. Valente, L. Papini, A. Formentini, C. Gerada, and P. Zanchetta, "Radial Force Control of Multisector Permanent-Magnet Machines for Vibration Suppression," *IEEE Tran. on Industrial Electronics*, vol. 65, no. 7, pp. 5395–5405, 2017.
[24] J. Chen, Y. Qin, A. M. Bozorgi, and M. Farasat, "Low Complexity Dual-Vector Model Predictive Current Control for Surface-Mounted Permanent Magnet Synchronous Motor Drives," *IEEE Journal of Emerging and Selected Topics in Power Electronics*, 2019.
[25] M. Khalilzadeh and S. Vaez-Zadeh, "Computation Efficiency and Robustness Improvement of Predictive Control for PMS Motors," *IEEE Journal of Emerging and Selected Topics in Power Electronics*, 2019.
[26] B. Hu, L. Kang, J. Cheng, X. Luo, and Z. Zhang, "Model Predictive Power Control with Dual Vectors for Three-level Inverter," *IEEE Journal of Emerging and Selected Topics in Power Electronics*, 2019.
[27] L. Serrano-Iribarnegaray, "Space phasor theory and control of multiphase machines through their decoupling into equivalent three-phase machines," *Electrical Engineering*, vol. 96, no. 1, pp. 79–94, 2014.
[28] Atan2, https://en.wikipedia.org/wiki/Atan2. Accessed: 12/06/2019 .
[29] F. Meier, "Permanent-Magnet Synchronous Machines with Non-Overlapping Concentrated Windings for Low-Speed Direct-Drive Applications," Ph.D. dissertation, KTH, 2008.
[30] EMETOR, https://www.emetor.com. Accessed: 12/06/2019 .
[31] E. Severson, S. Gandikota, and N. Mohan, "Practical Implementation of Dual-Purpose No-Voltage Drives for Bearingless Motors," *IEEE Tran. on Industry Applications*, vol. 52, no. 2, pp. 1509–1518, March 2016.
[32] T. I. Baumgartner, "A Magnetically Levitated 500 000 rpm Electrical Drive System," Ph.D. dissertation, ETH Zurich, 2013.
[33] K. Raggl, T. Nussbaumer, and J. W. Kolar, "A Comparison of Separated and Combined Winding Concepts for Bearingless Centrifugal Pumps," *Journal of power electronics*, vol. 9, no. 2, pp. 243–258, 2009.
[34] S. Silber, W. Amrhein, P. Bosch, R. Schob, and N. Barletta, "Design Aspects of Bearingless Slice Motors," *IEEE/ASME Tran. on Mechatronics*, vol. 10, no. 6, pp. 611–617, 2005.
[35] Frobenius Inner Product, https://en.wikipedia.org/wiki/Frobenius_inner_product. Accessed: 12/06/2019 .
[36] S. Skogestad and I. Postlethwaite, *Multivariable Feedback Control: Analysis and Design*. Wiley New York, 2007, vol. 2.
[37] S. N. Vukosavic, *Digital Control of Electrical Drives*. Springer Science & Business Media, 2007.
[38] K. Meessen, J. Paulides, and E. Lomonova, "Force Calculations in 3-D Sylindrical Structures Using Fourier Analysis and the Maxwell Stress Tensor," *IEEE Tran. on Magnetics*, vol. 49, no. 1, pp. 536–545, 2012.

Spasoje Mirić (S'13) received the B.Sc. and M.Sc. degrees in electrical engineering in 2012 and 2013, respectively, from the University of Belgrade, Belgrade, Serbia. He is currently working towards his Ph.D. degree in electrical engineering at the Swiss Federal Institute of Technology (ETH) Zurich, Zurich, Switzerland. His research interests are novel electrical machine topologies, linear machines and bearingless motors for highly dynamic actuator systems.

Rosario V. Giuffrida (S'19) received the B.Sc. degree in electronics engineering in 2016 from the University of Catania, Italy and the M.Sc. degree in Robotics, Systems and Control in 2019 from the Swiss Federal Institute of Technology (ETH) Zurich, Switzerland. Currently, he is with the Power Electronic Systems Laboratory at ETH Zurich for his Ph.D. studies. His research interests focus on design, sensing and motion control concepts for novel magnetically levitated actuators.

Dominik Bortis (M'08) received the M.Sc. and Ph.D. degree in electrical engineering from the Swiss Federal Institute of Technology (ETH) Zurich, Switzerland, in 2005 and 2008, respectively. In May 2005, he joined the Power Electronic Systems Laboratory (PES), ETH Zurich, as a Ph.D. student. From 2008 to 2011, he has been a Postdoctoral Fellow and from 2011 to 2016 a Research Associate with PES, co-supervising Ph.D. students and leading industry research projects. Since January 2016 Dr. Bortis is heading the research group Advanced Mechatronic Systems at PES, which concentrates on ultra-high speed motors, magnetic bearings and bearingless drives, new linear-rotary actuator and machine concepts with integrated power electronics. In this context, multi-objective optimizations concerning weight/volume/efficiency/costs, the analysis of interactions of power electronics and electric machines, and EMI are given special attention. Targeted applications include advanced industry automation and manufacturing, e.g. highly dynamic and precise positioning systems, medical and pharmaceutical systems, e.g. ultra-high purity and blood pumps, and future mobility concepts, including motors and actuators for hybrid and electric vehicles, more electric aircraft and satellites. Dr. Bortis has published more than 90 scientific papers in international journals and conference proceedings. He has filed 32 patents and has received 6 IEEE Conference Prize Paper Awards.

Johann W. Kolar (F'10) received the M.Sc. and Ph.D. degree (summa cum laude / promotio sub auspiciis praesidentis rei publicae) from the University of Technology Vienna, Austria, in 1997 and 1999, respectively. Since 1984, he has been working as an independent researcher and international consultant in close collaboration with the University of Technology Vienna, in the fields of power electronics, industrial electronics and high performance drive systems. He has proposed numerous novel PWM converter topologies, modulation and control concepts and has supervised 70+ Ph.D. students. He has published 880+ scientific papers in international journals and conference proceedings, 4 book chapters, and has filed 190+ patents. The focus of his current research is on ultra-compact and ultra-efficient SiC and GaN converter systems, wireless power transfer, solid-state transformers, power supplies on chip, and ultra-high speed and bearingless motors. Dr. Kolar has received 28 IEEE Transactions and Conference Prize Paper Awards, the 2014 IEEE Middlebrook Award, the 2016 IEEE William E. Newell Power Electronics Award, the 2016 IEEE PEMC Council Award and two ETH Zurich Golden Owl Awards for excellence in teaching. He initiated and/or is the founder of four ETH Spin-off companies. He is a member of the steering committees of several leading international conferences in the field and has served from 2001 through 2013 as an Associate Editor of the IEEE Transactions on Power Electronics. Since 2002 he also is an Associate Editor of the Journal of Power Electronics of the Korean Institute of Power Electronics and a member of the Editorial Advisory Board of the IEEJ Transactions on Electrical and Electronic Engineering.